

DYNAMIC MODELING OF A HARD DISK DRIVE
ACTUATOR USING SUB-COMPONENT FINITE
ELEMENT MODELS AND MODAL
SUPERPOSITION

By

JEFFREY DON ANDRESS

Bachelor of Science

Oklahoma State University


Stillwater, Oklahoma

1993

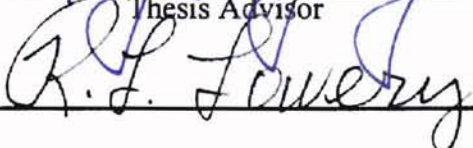
Submitted to the Faculty of the
Graduate School of the
Oklahoma State University
in partial fulfillment
of the requirements for
the Degree of
MASTER OF SCIENCE
May, 2000


DYNAMIC MODELING OF A HARD DISK DRIVE
ACTUATOR USING SUB-COMPONENT FINITE
ELEMENT MODELS AND MODAL
SUPERPOSITION


Thesis Approved:



Thesis Advisor







Dean of the Graduate College

PREFACE

The purpose of this study was to develop a methodology whereby complex structures, such as hard disk drive head stack assemblies, can be modeled accurately in a compact form. The head stack assembly was divided into three sub-components, the yoke/coil, the actuator arm, and the suspension. Finite element models of each sub-component were created to provide the natural frequencies and corresponding mode shapes of the individual sub-components. Coupling terms were then derived that describe how the sub-components interact to form the overall system dynamics. The resulting sub-component finite element analytical model was a 15 degree of freedom model that could quickly be solved using commercially available matrix manipulation software. The model proved to be accurate in predicting the off-track motion of the head stack assembly and helped provide understanding as to which resonances are the most detrimental to drive performance. Initial simulations showed that some of the boundary conditions and assumptions used in creating the sub-component finite element models were incorrect. However, by comparing the model results to measured data, the sub-component finite element analytical model provided direction to improve the accuracy of the sub-component finite element models.

I would like to thank Mr. Roy Wood and Mr. John Stricklin who provided valuable insight and assistance study. Without their knowledge and advice, this research would not have been possible.

TABLE OF CONTENTS

Chapter	Page
1 Introduction	1
2 Background	8
3 Model Development	12
3.1 Background Theory	12
3.2 HSA Model Development	20
3.2.1 Development of the Mass and Stiffness Matrices of the Un-damped System	22
3.2.2 Development of the Force Input Vector	26
3.2.3 HSA Modeling Assumptions	30
3.2.4 HSA Model Discussion	32
3.2.5 State Space Representation of the HSA Model	35
4 Finite-Element Models	37
4.1 Full HSA Finite-Element Model	37
4.2 Sub-Component FE Models	39
4.2.1 Suspension FE Model	40
4.2.2 Actuator Arm FE Model	42
4.2.3 Yoke and Coil FE Model	44
4.3 Experimental Verification of the FE Models	46
5 HSA Model Simulation Results and Discussion	48
5.1 Reduced Order Model Simulation	48
5.2 Full Order Model Simulation	54
6 Conclusions and Future Work	61
6.1 Conclusions	61
6.2 Future Work	62
REFERENCES	64
APPENDIX A	66

Chapter	Page
APPENDIX B	69
APPENDIX C	72
APPENDIX D	75

LIST OF TABLES

Table	Page
Table 4-1: Suspension FE Model vs. Measured Natural Frequencies	42
Table 4-2: Actuator Arm FE Model vs. Measured Natural Frequencies	44
Table 4-3: Yoke/Coil FE Model vs. Measured Natural Frequencies	45

LIST OF FIGURES

Figures	Page
Figure 1-1: Head Stack Assembly (HSA)	3
Figure 1-2: Block Diagram of Control System	4
Figure 3-1: HSA Model	21
Figure 3-2: Forces due to Current Input to the Coil	28
Figure 4-1: Full HSA FE Model	37
Figure 4-2: HSA FE Model vs. Measured Mechanical Transfer Function	39
Figure 4-3: Suspension Sub-Component FE Model	41
Figure 4-4: Actuator Arm Sub-Component FE Model	42
Figure 4-5: Yoke/Coil Sub-Component FE Model	44
Figure 5-1: Rigid Body State Space Model vs. Measured Frequency Response	49
Figure 5-2: Translational and Rotational Components of the State Space Model	50
Figure 5-3: Corrected State Space Model vs. Measured Frequency Response	51
Figure 5-4: Non-Collocated Transfer Function vs. Measured Frequency Response	53
Figure 5-5: Initial Simulation of the Sub-Component FE Analytical Model	55
Figure 5-6: Sub-Component FE Model Simulation with Corrected Sway Mode Coupling Factors	56

Figures	Page
Figure 5-7: Original Suspension 3 rd Bending Mode	58
Figure 5-8: Modified Suspension 3 rd Bending Mode	58
Figure 5-9: Modified Sub-Component FE Analytical Model Simulation	59
Figure A-1: Suspension 1 st Bending	67
Figure A-2: Suspension 1 st Torsion	67
Figure A-3: Suspension 2 nd Bending	67
Figure A-4: Suspension 2 nd Torsion	67
Figure A-5: Suspension 3 rd Bending	68
Figure A-6: Suspension Sway	68
Figure B-1: Arm 1 st Bending	70
Figure B-2: Arm Sway	70
Figure B-3: Arm 2 nd Bending	70
Figure B-4: Arm 1 st Torsion	71
Figure C-1: Yoke/Coil 1 st Bending	73
Figure C-2: Yoke/Coil 1 st Torsion	73
Figure C-3: Yoke/Coil Sway	74

NOMENCLATURE

$\{A\}$	Normalized mode shape vector
$[A]$	State space system matrix
$[B]$	State space input matrix
$[C]$	State space output matrix
$[C_{damp}]$	Damping matrix
$[D]$	State space direct transmission matrix
$\{F\}$	Input force vector
Γ	Modal participation factor
I	Current (Amp)
J_B	Mass moment of inertia of the rigid actuator body (lbf-in-s ²)
J_T	Total mass moment of inertia of the HSA about the pivot center (lbf-in-s ²)
K	Sub-component finite element model element stiffness
$[K]$	Stiffness Matrix
$K_{adjustment}$	Adjustment gain required to correct the error in the state space model
$K_{bearing}$	Pivot bearing stiffness (lbf/in)
K_{BW}	Gain factor associated with the drive electronics
K_θ	DC gain of the rotational component transfer function
K_t	Voice coil motor torque constant (oz-in/Amp)
K_{Trans}	DC gain of the translational component transfer function

l	Moment arm from pivot center to lumped nodal mass (in.)
$[M]$	Mass matrix
m	Sub-component finite element model lumped nodal mass
m_B	Mass of the rigid actuator body (lbf-s ² /in)
M_e	Effective mass
mk	Modal stiffness
mm	Modal mass
m_{ST}	Total mass of the suspension sub-component FE model (lbf-s ² /in)
M_T	Total mass of the HSA (lbf-s ² /in)
m_T	Total mass of the sub-component FE model (lbf-s ² /in)
$\{\phi\}$	Mode shape vector normalized by the square root of the modal mass
q	Modal coordinate
R_c	Moment arm from pivot center to active length center (in.)
R_h	Moment arm from pivot center to slider (in.)
$rmcf$	Rotational to modal coupling factor
ω	Natural frequency (Rad/s)
$\{y\}$	State variable vector
ξ	Damping ratio

1 Introduction

As society continues to demand accurate and timely information, the need to quickly and reliably store and retrieve data is ever increasing. To date, rigid, magnetic disk drives have become the primary data storage devices in today's computer systems. Disk drives are now used in desktop computers, workstations, and servers as well as portable devices such as notebook computers and digital cameras. As the applications in which disk drives are used continue to expand, disk drive users constantly demand increased storage capacity and improved drive performance while insisting that drive manufacturers maintain or decrease the physical size of the drive. To keep pace with the demand for storage capacity, the current trend in the disk drive industry is a doubling of capacity each year.

For drive dimensions to remain unchanged or even decrease, drive manufactures must be able to write more data on a given surface to meet the growing capacity demand. Increasing the storage capacity of a drive therefore requires increasing the bits per square inch (areal density) that are written on a disk surface. Areal density is the product of bits per inch (BPI) and tracks per inch (TPI). BPI is defined as the number of bits that can be written along an inch of data track in the circumferential direction, while TPI is defined as the number of data tracks that can be written on an inch of the disk surface in the radial direction. The width of a data track is the reciprocal of TPI. For example a 100 micro-inch wide data track corresponds to 10,000 TPI. At 10,000 TPI approximately 40

data tracks could be written on the edge of a standard piece of white paper (standard white paper is approximately 0.004 inches thick). While BPI is limited mainly by the fly height of the read/write head above the disk surface, TPI is limited by the track following servo system. It is becoming increasingly hard for drive manufacturers to increase the BPI, such that increased track densities are accounting for a larger percentage of the annual areal density growth rate.

The limitations of the servo system are defined by the flexibility of the mechanical components as well as the controller design. The flexibility of the mechanical components can adversely affect drive performance in two ways. First, as TPI increases, drives become increasingly susceptible to mechanical resonances that cause the read/write head to move off-track, since the displacement of the head becomes an increasing percentage to the total track width. Second, to compensate for the TPI increase, the drive bandwidth must increase to maintain the drive's ability to track accurately in the presence of external shock and vibration disturbances. However, as the drive bandwidth increases, the stability of the servo loop is threatened due to the mechanical resonances of the drive, since increasing the bandwidth of the drive can decrease the gain margin of mechanical resonances. Resonances that were previously ignored due to insufficient amplitude to be of interest can become stability issues if they are not raised in frequency or reduced in amplitude.

One way to categorize drive resonances is by how they are excited and what performance specifications they affect. Using this criterion, drive resonances can be split into two categories, in-the-loop and out-of-the-loop. In-the-loop resonances are resonances that modify the open loop or structural response and are excited by control

inputs to the actuator coil. In-the-loop resonances are typically head stack assembly

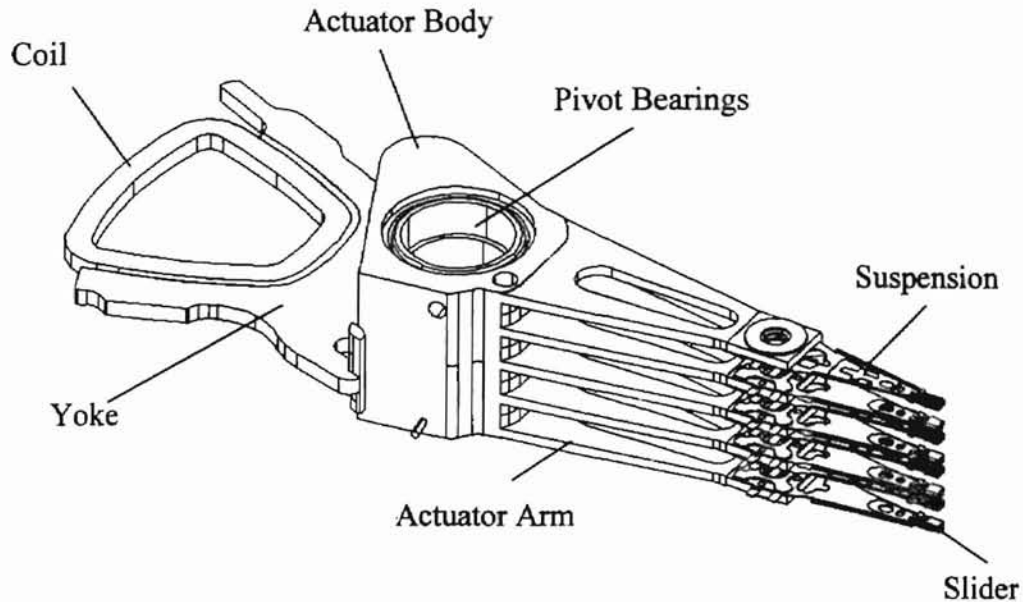


Figure 1-1: Head Stack Assembly (HSA)

(HSA) resonances, which include actuator arm, suspension, pivot bearing, and yoke/coil resonances. Figure 1-1 shows a typical HSA. Out-of-the-loop resonances are all other resonances that do not directly modify the open loop or structural response since they are not directly excited by the servo loop and the dynamic positioning of the HSA. Out-of-the-loop resonances include disk pack, basedeck and topcover resonances that can be excited by windage forces generated by the rotating disks, external shock and vibration excitations, and spindle motor bearing defects. These types of resonances can be considered error excitations to the system.

As TPI continue to increase to meet the growing capacity demand and servo bandwidths increase to help maintain drive performance margins, each generation of drive becomes increasingly susceptible to drive resonances. In-the-loop HSA resonances are the cause of significant servo stability and performance problems since

they modify the open loop response. The open loop response is a combination of the servo system and mechanical system transfer functions as shown in Figure 1-2. The mechanical

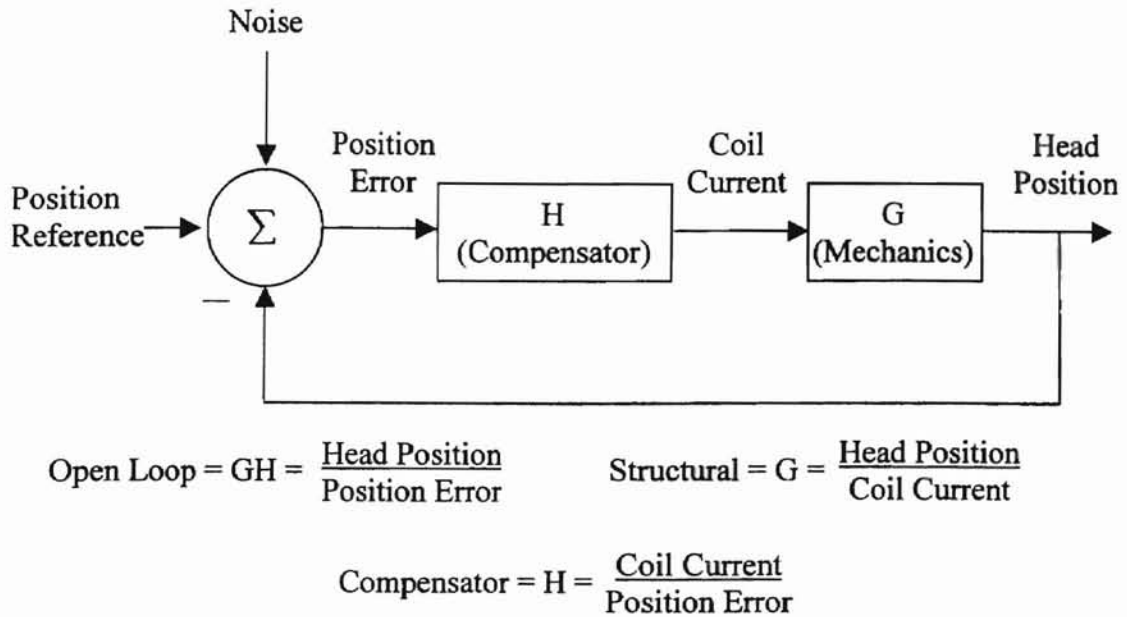


Figure 1-2: Block Diagram of Control System

transfer function of the HSA relates coil current input to displacement of the slider. Any significant deformation of the HSA due to resonances of the yoke/coil, arms, suspension, and pivot bearings can therefore adversely modify the open loop response. The ability to accurately model the HSA in order to predict the effects of HSA resonances on drive performance would be a valuable tool to both the servo and mechanical drive design engineers. Such a model would give servo engineers the ability to design track following loops to compensate for the mechanical resonances and would give mechanical engineers the ability to optimize the actuator design to reduce the impact of HSA resonances on the servo system in advance of a working drive.

The HSA is a complex structure made up of several sub-components (yoke, coil, pivot bearing, actuator body, actuator arms, and suspensions) as shown in Figure 1-1. Typically, the dynamic behavior of complex structures such as HSAs can be modeled effectively using finite element (FE) models. In order to accurately predict the off-track displacement of the slider due to coil current input, the entire HSA (all sub-components) must be modeled and correct boundary conditions must be applied. As a result, the full HSA FE model can become very large, on the order of 120,000 degrees-of-freedom (DOF). FE models of this magnitude take numerous hours, even days, to develop and solve, and can become cumbersome to work with. The goal of a HSA FE model is not just to predict natural frequencies and mode shapes of HSA resonances, but to provide a tool whereby the actuator design can be optimized to meet performance specifications and reduce the impact of resonances on drive performance. However, if a full HSA FE model is used, the model development time, solve time, and size are not conducive to the numerous iterations that might be necessary to arrive at an optimal design, thereby, reducing the usefulness of the full FE model as a design tool.

Due to the complexity and size of the full HSA FE model, a smaller, more compact alternative would be preferred. The goal of providing this alternative without the size and complexity of the FE model would most likely be achieved through the development of an analytical model. As opposed to the thousands of DOF associated with the full HSA FE model, the DOF of an analytical model would be limited to the number of modeled resonances. There are numerous mechanical resonances of the HSA, however, only resonances that cause off-track displacements of the slider are of concern. Thus, the analytical model could be reduced to approximately 15 DOF which would include

rigid body, yoke/coil, arm, suspension, and pivot bearing modes. Analytical models can be expressed in a state-space form, which, can easily be solved by matrix operation software such as Matlab in seconds as opposed to the hours required to solve the FE model. Because of the compact size of the analytical model (15 DOF compared to 120,000 DOF for the analytical and FE models respectively), the analytical model can be used to quickly and efficiently optimize the actuator design to provide improved HSA dynamics. However, when analytical models are developed, the mechanical structure being modeled is generally simplified such that the results of the model may not be accurate or may not include higher order modes that are of interest. Since the HSA is a complex structure, the assumptions and simplifications needed to create an analytical model limit the accuracy of the model to approximately 6 kHz. The TPI, drive bandwidths, sample-rates, and system dynamics of today's drives require that the HSA model be able to accurately predict the off-track performance up to 15 kHz. There are numerous HSA resonances above 6 kHz that significantly affect drive performance and servo stability that are difficult to model accurately by means of an analytical model.

The disadvantages of both the FE and analytical HSA models limit the usefulness of both methods in the prediction of HSA dynamics on drive performance. The limitations of these modeling methods also prevent both the FE and analytical models from being useful design tools in the optimization of the actuator to meet performance specifications and reduce the impact of drive resonances on servo stability. Therefore, the need exists for a model that can accurately predict the dynamics of complex structures yet provide the model in a compact form that can be quickly and easily solved. The complexity of the HSA, however, requires the use of FE models to accurately

predict natural frequencies and mode shapes of the structure. The size, complexity, development time, and solve time of the FE model can be reduced if sub-components, instead of the entire HSA, are modeled. If boundary conditions are modeled correctly, sub-component FE models of the HSA can provide the natural frequencies and mode shapes with the same accuracy of the full HSA model. The modal information obtained from the sub-component FE model can be combined into a compact analytical model by using mode summation techniques and by deriving the coupling equations that describe how the sub-components interact. The resultant model is a compact model (15 DOF like the analytical model) that can accurately describe the complex dynamics of the HSA. The coupling of the sub-components describe how the flexibilities of the system interact. The sub-component FE analytical model can therefore provide directions for improving the mechanics to reduce the resonance impact on drive performance.

The objective of the research described in this thesis is to develop the methodology whereby complex structures, such as a hard disk drive HSA, can be modeled accurately in a compact form. This study will detail the development of a compact HSA model that can predict the dynamic performance of the drive while track following. The details of modeling and combining the servo system and HSA mechanical models are not addressed in this paper since there are several papers in the open literature concerning this subject matter.

2 Background

Little has been found in published literature concerning model development of disk drive head stack assemblies. Currently, the majority of this research is being performed by individual drive design companies or is funded by the disk drive industry and, therefore, remains proprietary. However, there have been several papers published recently that develop models to predict the track following and disturbance rejection capabilities of the servo system. These papers develop and discuss methods for creating full HSA models, as the mechanical resonances of the HSA significantly impact drive performance and servo stability.

Radwan and Whaley [13] investigated how the mechanical flexibilities of a disk drive interact with the servo system and were also able to demonstrate the capability to predict both an open loop frequency response and the off-track performance of the HSA due to operating vibration excitations. Through this research, Radwan and Whaley developed a full FE model, which can be utilized to calculate the mechanical frequency response of the HSA. Using this full FE model, a modal analysis was performed and then the corresponding frequency response function due to a harmonic force input to the coil was calculated. The plot of the frequency response was then copied to an ASCII file and imported to MathCAD where a transfer function of the servo system was added, resulting in the open loop transfer function of the system. While good correlation between measured and modeled data was achieved, the process of obtaining

the mechanical transfer function was difficult. The data that was imported to MathCAD was not a model of the HSA but was simply the magnitude and phase versus frequency data points obtained from the FE harmonic analysis. Thus, if any structural modifications were to be considered, the entire process starting with the full FE model of the HSA would have to be repeated.

In Radwan et al. [11], the use of FE models to predict a drive's track following capability was further refined. Instead of simply exporting a transfer function graph representing the HSA mechanical response, the full FE model was reduced to a state space representation of the HSA. The state-space HSA model was then combined with a model of the servo system and MATLAB was used to solve for the open loop response. The state space HSA model was created by first performing a modal analysis on the full FE model. Nodal displacements at both the excitation and response nodes (a node on the coil and a node on the slider respectively) from each mode shape were extracted from the FE solution. The modal mass and natural frequency for each mode was also extracted. Each mode was then modeled as a single DOF system with the total system response the superposition of the individual modes. Not all modes were used in the state space model. Only modes that had significant contribution in the off-track direction were used in the modal sum. The benefits of this second model are that Radwan et al. developed a method to reduce a detailed FE model of the HSA to a set of state space equations. They also demonstrated that the off-track response of the FE model can be approximated by the superposition of a reduced number of modes. However, like the first work, the model was ultimately reliant on a full detailed FE model of the HSA.

While the two previous models discussed above dealt with the use of detailed FE HSA models, a few examples of analytical HSA models can be found in the literature. As previously mentioned, the complex nature of the HSA requires that the mechanical structure be simplified in order to develop an analytical model. The simplifications needed to create an analytical HSA model restrict the model's usefulness. While assumptions and approximations can be made that allow first order modes to be predicted, higher order modes of the system would be in error. Thus the use of analytical models is limited. Radwan et al. [12] provides an example of a simplified analytical model in order to predict track following performance under external shock and vibration excitations. However, only the rigid body dynamics of the actuator were modeled and mechanical resonances were not considered. Because mechanical resonances were not considered, the frequency response of the model is valid for only a few hundred hertz. The model presented by Radwan et al. is therefore useful only for the investigation of the low frequency response of the actuator to external excitations.

The HSA model presented by Ono and Teramoto [10] expands the useful frequency range of the model presented by Radwan et al. by including the flexibility of the pivot bearings. The model presented by Ono and Teramoto was developed to provide understanding of the interaction between the rigid body rotational mode of the actuator and the flexible mode of the pivot bearings. While the model developed was adequate for their study, the Ono and Teramoto model did not include flexible modes of the yoke/coil, actuator arms, or suspensions. These modes must be included if the model is to be used to understand the dynamic effects of the HSA on the servo system.

Aruga et al. [1] modeled the HSA as a 3 DOF system, including the rigid body rotational mode, a pivot bearing mode, and one arm mode. Their study dealt with the design of a new concept actuator meant to reduce the off-track impacts of the fundamental pivot-bearing mode. The Aruga et al. model is still too simplified for today's disk drives and servo systems. There are several detrimental suspension, arm, and yoke modes that must be accounted for in order to predict drive performance and servo stability.

The models and methods detailed in the open literature are either too complicated (full FE HSA models) or too simplified (analytical models), resulting in limited use in the prediction of HSA dynamics on drive performance. The limitations of these modeling methods also prevent the models from serving as useful design tools for drive design engineers, who must optimize the actuator to meet performance goals while reducing the impact of resonances on servo stability. This study will detail the development of a compact model that can be used to predict the dynamic performance of complex structures such as HSAs.

3 Model Development

3.1 Background Theory

A multi-degree-of-freedom system can be described by a set of n simultaneous second order differential equations. In matrix form, the equations are expressed as

$$[M]\{\ddot{y}\} + [C_{damp}]\{\dot{y}\} + [K]\{y\} = \{F(t)\} \quad (3-1)$$

The general solution to equation (3-1) is the sum of the complementary function and the particular integral. The complementary function satisfies the homogeneous differential equation (right side of the equation equals zero) which physically corresponds to the free vibration problem ($\{F(t)\} = 0$). Under free vibration, the system is not subjected to any external excitation and its motion is governed only by the initial conditions. When the excitation source is harmonic ($\{F(t)\} = \{F_0 \sin \omega t\}$), the solution to the particular integral is the steady state oscillation of the system at the same frequency ω as the excitation. Seldom is it necessary to determine the motion of a system under conditions of free vibration. However, the analysis of a system in free vibration provides two important dynamic properties of the system: the natural frequencies of the system and the corresponding mode shapes. For a multi-degree-of-freedom system with n degrees-of-freedom (DOF), there are n natural frequencies and mode shapes. Finite element modeling software is often used to calculate the natural frequencies and mode shapes for complicated systems with many degrees-of-freedom.

If the effects of damping do not influence the natural frequencies of the system, when solving equation (3-1) for the free vibration case, the damping term is usually omitted. For the undamped free vibration problem, equation (3-1) reduces to

$$[M]\{\ddot{y}\} + [K]\{y\} = \{0\} \quad (3-2)$$

For free vibrations of the undamped structure, $\{y\}$ is of the form

$$y_i = A_i \sin(\omega t + \psi) \quad i = 1, 2, \dots, n$$

or in vector notation

$$\{y\} = \{A\} \sin(\omega t + \psi) \quad (3-3)$$

where A_i is the displacement amplitude of the i^{th} coordinate and n is the number of DOF.

Substituting equation (3-3) into equation (3-2) gives

$$[[K] - \omega^2[M]]\{A\} = 0 \quad (3-4)$$

which is a set of n homogeneous linear algebraic equations in $\{A\}$ with n unknown displacements A_i and an unknown parameter ω^2 . The nontrivial solution to equation (3-4) requires that the determinant of the coefficient matrix ($[[K] - \omega^2[M]]$) equal zero.

Equating the determinant to zero gives the characteristic equation

$$\det[[K] - \omega^2[M]] = 0 \quad (3-5)$$

from which the natural frequencies of the system are found. In general, equation (3-5) results in a polynomial equation of degree n in ω^2 which is satisfied by n values of ω^2 , where

$$\omega_i \quad i = 1, 2, \dots, n$$

are the natural frequencies of the system and n is the number of DOF. Since equation (3-4) is a homogeneous system of linear equations and the determinant of the coefficient matrix is zero, the equations are linearly dependent such that there are an infinite number of solutions for $\{A\}$. Thus, for each natural frequency ω_i which satisfies equation (3-5), there is not a unique solution for the corresponding displacement amplitude vector $\{A\}$. Typically, one of the displacement amplitudes in the amplitude vector $\{A\}$ is assigned a unit value, although any number is sufficient. By substituting each of the natural frequencies into equation (3-4), the corresponding amplitude vector $\{A\}$ can be calculated relative to the arbitrarily chosen element. These ratio values are known as the mode shape or modal vector for a particular natural frequency. The mode shape is often referred to as a normal mode since the elements in the vector $\{A\}$ have been normalized by an arbitrary value. Since there are n natural frequencies, there will be n corresponding normalized mode shape vectors.

The normal modes may be conveniently arranged in the columns of a matrix known as the modal matrix where each column represents a mode shape associated with a particular natural frequency. For the general case of an n DOF system, the modal matrix is written as

$$[A] = [\{A\}_1 \{A\}_2 \dots \{A\}_n]$$

or

$$[A] = \begin{bmatrix} A_{11} & A_{12} & \dots & A_{1n} \\ A_{21} & A_{22} & \dots & A_{2n} \\ \vdots & \vdots & \ddots & \vdots \\ A_{n1} & A_{n2} & \dots & A_{nn} \end{bmatrix} \quad (3-6)$$

For an n DOF system, each natural frequency has its own mode shape and behaves essentially as a single DOF system. The total motion of the system, the solution to equation (3-2), is the superposition of the normal modes of the system.

$$\{y\} = \{A\}_1 C_1 \sin(\omega_1 t + \psi_1) + \{A\}_2 C_2 \sin(\omega_2 t + \psi_2) + \dots + \{A\}_n C_n \sin(\omega_n t + \psi_n) \quad (3-7)$$

where the C 's and ψ 's are arbitrary constants of integration that are determined by the initial conditions of the system.

An interesting property of the normal modes of a system is that they are orthogonal with respect to the mass and stiffness matrices. The orthogonal nature of the normal modes is defined as follows

$$\{A\}_i^T [M] \{A\}_j = 0 \quad \text{for } i \neq j \quad (3-8)$$

$$\{A\}_i^T [K] \{A\}_j = 0 \quad \text{for } i \neq j \quad (3-9)$$

and

$$\{A\}_i^T [M] \{A\}_i = mm_i \quad i = 1, 2, \dots, n \quad (3-10)$$

$$\{A\}_i^T [K] \{A\}_i = mk_i \quad i = 1, 2, \dots, n \quad (3-11)$$

where mm_i and mk_i are defined as the modal mass and modal stiffness of the i^{th} mode.

The resulting modal mass and modal stiffness matrices are diagonal.

As previously mentioned, the amplitudes of vibration for normal modes are only relative values which may be scaled or normalized to an arbitrary value. It is often convenient to normalize the mode shapes by the square root of the modal mass.

$$\phi_{ij} = \frac{A_{ij}}{\sqrt{\{A\}_i^T [M] \{A\}_i}} \quad \text{or} \quad \phi_{ij} = \frac{A_{ij}}{\sqrt{mm_i}} \quad (3-12)$$

where ϕ_j is the modal mass normalized i^{th} component of the j^{th} modal vector. The modal matrix can be re-written as

$$[\phi] = \begin{bmatrix} \phi_{11} & \phi_{12} & \cdots & \phi_{1n} \\ \phi_{21} & \phi_{22} & \cdots & \phi_{2n} \\ \vdots & \vdots & \ddots & \vdots \\ \phi_{n1} & \phi_{n2} & \cdots & \phi_{nn} \end{bmatrix} \quad (3-13)$$

Substituting $\{\phi\}_i$ for $\{A\}_i$ in equation (3-8) through (3-11) results in

$$\{\phi\}_i^T [M] \{\phi\}_j = 0 \quad \text{for } i \neq j \quad (3-14)$$

$$\{\phi\}_i^T [K] \{\phi\}_j = 0 \quad \text{for } i \neq j \quad (3-15)$$

$$\{\phi\}_i^T [M] \{\phi\}_i = 1 \quad i = 1, 2, \dots, n \quad (3-16)$$

$$\{\phi\}_i^T [K] \{\phi\}_i = \omega_i^2 \quad i = 1, 2, \dots, n \quad (3-17)$$

The advantage of this normalization method will be shown below in equation (3-23).

The equations of motion represented in equation (3-2) are generally coupled through the mass and/or the stiffness matrices. Dynamic coupling exists if the mass matrix is non-diagonal where as static coupling exists if the stiffness matrix is non-diagonal. If the equations are uncoupled by the proper choice of coordinates, each equation can be solved independently of the others and each mode can then be examined as an independent single-DOF system. Although it is always possible to de-couple the equations of motion for the un-damped system, it is not always possible to de-couple damped systems. Due to the orthogonal properties of the modal matrix, the modal matrix, equation (3-6) or equation (3-13), can be used to de-couple the mass and stiffness matrices in equation (3-2). To de-couple the mass and stiffness matrices, a modal coordinate q_i is defined such that

$$\{y\} = \sum_{i=1}^n \{\phi\}_i q_i \quad (3-18)$$

Substituting equation (3-18) into equation (3-2) and pre-multiplying by $[\phi]^T$ gives

$$\{\phi\}_i^T [M] \{\phi\}_i \{\ddot{q}\} + \{\phi\}_i^T [K] \{\phi\}_i \{q\} = 0 \quad (3-19)$$

However, from equations (3-8), (3-9), (3-16) and (3-17), equation (3-19) reduces to a set of n de-coupled equations of the form

$$\ddot{q}_i + \omega_i^2 q_i = 0 \quad (3-20)$$

So far, damping terms have been ignored. As previously mentioned, when damping is considered, it is not always possible to de-couple the equations of motion. If, however, the damping matrix $[C]$ is proportional to the mass $[M]$ and/or stiffness $[K]$ matrix, the following hold true

$$\{\phi\}_i^T [C] \{\phi\}_j = 0 \quad \text{for } i \neq j \quad (3-21)$$

and

$$\{\phi\}_i^T [C] \{\phi\}_i = 2\zeta_i \omega_i \quad \text{for } i = 1, 2, \dots, n \quad (3-22)$$

so that equation (3-20) becomes

$$\ddot{q}_i + 2\zeta_i \omega_i \dot{q}_i + \omega_i^2 q_i = 0 \quad (3-23)$$

In equation (3-23), each mode is expressed as a single-DOF system where the total system response is the superposition of the contributing modes (equation (3-18)). The advantage of equation (3-23) is that an n -DOF system can be represented in terms of the modal parameters of the system without the knowledge of the mass and stiffness

matrices. As previously mentioned, the modal parameters, such as the natural frequencies and mode shapes, of complex systems can be determined from FE models. Equations (3-23) and (3-18) allow a FE model of a complex system to be reduced to a set of n single-DOF equations, where n is the number of flexible modes considered, by first solving the FE model for the natural frequencies and mode shapes of the system. The mass and stiffness matrices generated by the FE software can be extremely large (the mass and stiffness matrices will have as many rows and columns as there are DOF of the system), but are not needed to calculate the system response.

For lightly damped systems, such as HSAs, the damping terms in equation (3-23) serve mainly to limit the amplitude response at resonance. Appropriate damping terms for each mode can be determined experimentally by direct measurement or can be estimated by matching the resonant amplitudes from modeled and measured frequency response functions. For the HSA model that is being developed, the damping in the system is predominately due to structural damping such that ξ is generally assumed to be less than one percent.

As in free vibration, it is also possible to express the response of a system to forced vibration as the superposition of the normal modes. When the normal modes are used to de-couple the set of system equations, the modal superposition method reduces the problem of finding the response of a multi-DOF system to the determination of the response of n single-DOF systems. In forced vibration, the equations of motion are de-coupled by first solving for the natural frequencies (ω_i) and normalized mode shapes (ϕ) from the free vibration case. For the forced vibration condition, equation (3-23) becomes

$$\ddot{q}_i + 2\zeta_i \omega_i \dot{q}_i + \omega_i^2 q_i = f_i \quad (3-24)$$

where

$$f_i = \{\phi\}_i^T \{F\}$$

For systems with a large number of degrees of freedom, every mode may not significantly contribute or be of interest in the response of the system to forced excitation. Modal superposition allows the response of a system to be approximated by the sum of a limited number of normal modes thereby decreasing the number of degrees of freedom of the system.

The response of a system to ground or base motion is a specialized case of forced excitation. For an n -DOF system excited by base or ground motion, equation (3-24) can be re-written as

$$\ddot{q}_i + 2\zeta_i \omega_i \dot{q}_i + \omega_i^2 q_i = \Gamma_i \ddot{y}(t) \quad (3-25)$$

where the term

$$\Gamma_i = \frac{\sum_{j=1}^n m_j \phi_{ji}}{\sum_{j=1}^n m_j \phi_{ji}^2} \quad (3-26)$$

is called the modal participation factor and $\ddot{y}(t)$ is the motion of the ground. The modal participation factor relates how the ground motion excites a given mode. In equation (3-26), m_j is the actual mass value from the mass matrix $[M]$, associated with the j^{th} row and column. As previously mentioned, the differential equations of motion for a multi-DOF system are generally coupled through the mass and/or stiffness matrix. Equation (3-26) assumes that system of equations only exhibit static coupling such that the mass

matrix is diagonal and the equations are coupled through the stiffness matrix. When deriving the equations of motion for n -DOF system, the choice of the system coordinates will define the type of coupling. Just as a coordinate system can be found that decouples the system equations, a coordinate system can also be found that ensures only static coupling. From equation (3-16), the denominator of equation (3-26) is equal to one so that the modal participation factor becomes

$$\Gamma_i = \sum_{j=1}^n m_j \phi_{ji} \quad (3-27)$$

3.2 HSA Model Development

The goal of this thesis is to develop a compact model that can describe the dynamics of complex structures such as HSAs. The model that will be developed combines both FE and analytical modeling methods. In order to minimize the complexity, development time, and solve time that is often associated with FE models of complex structures, the HSA is divided into sub-components. The sub-component FE models can be developed and solved in less time compared to a full FE model of the HSA. The sub-component FE models provide the natural frequencies and mode shapes of the individual sub-components. In order to describe the complete system, coupling terms must be derived that describe how the sub-components interact to form the overall system dynamics.

Figure (3-1) shows a representation of the HSA used for the model development. In the model, only the off-track displacements of the various components are considered since it is the off-track motion that adversely effects drive performance. In the above

figure, the off-track direction is indicated by the y -axis. The HSA model consists of five

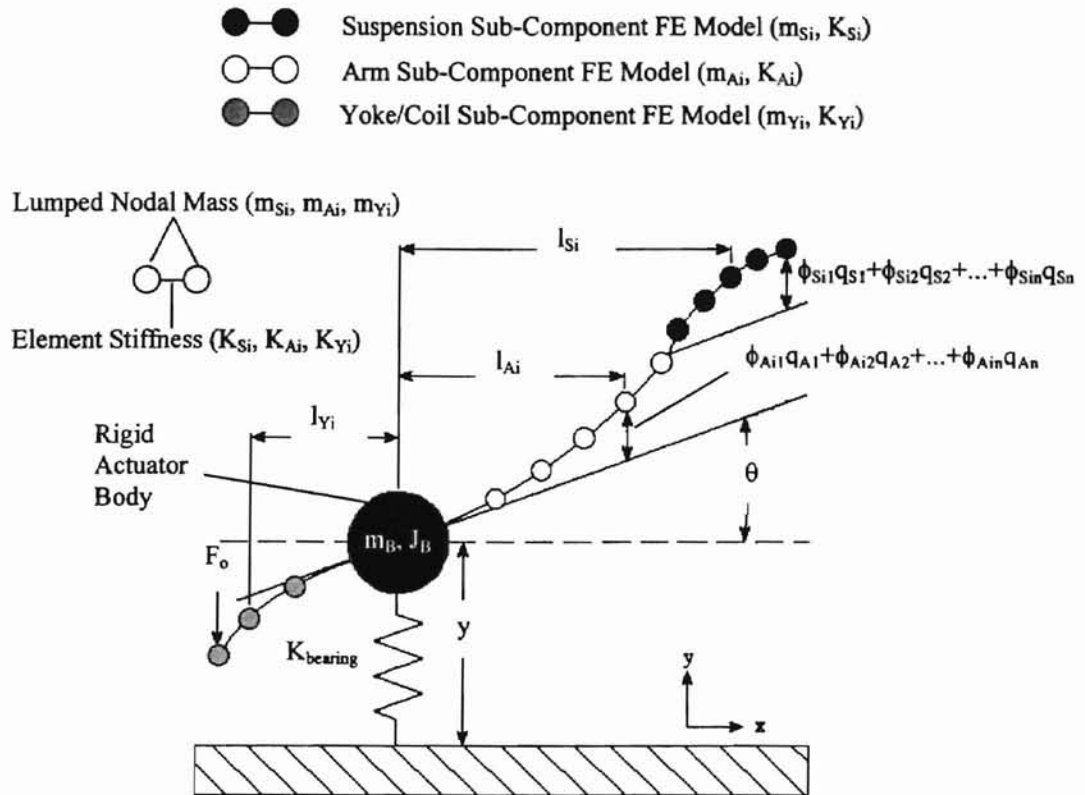


Figure 3-1: HSA Model

main parts: the yoke and coil, an actuator arm, a suspension, the actuator body, and the pivot bearings. The yoke/coil, actuator arm, and suspension are sub-component FE models. The actuator body is assumed to be rigid and the pivot bearings are modeled as a linear spring. Each sub-component FE model is represented by a series of masses and springs. In Figure (3-1) and the model development that follows, the subscripts S , A , and Y are used to identify parameters associated with the suspension, arm, and yoke/coil sub-component FE models respectively. The mass terms associated with the sub-component FE models (m_{Si} , m_{Ai} , and m_{Yi}) represent the lumped mass values at individual nodes and the spring terms (K_{Si} , K_{Ai} , K_{Yi}) represent the stiffness values of individual elements. The total displacement of each lumped mass is expressed as the sum of the rigid body

displacement, both translation and rotation, and the displacement due to the deformation of the sub-components.

$$\{y\}_{total} = \{y\}_{rigid} + \{y\}_{deformation} \quad (3-28)$$

The deformation in the off-track direction of each nodal lumped mass is obtained from the results of the corresponding sub-component FE model. Using modal superposition, the displacement due to deformation can be expressed in terms of the modal coordinates as the sum of the normal modes as in equation (3-18). Substituting equation (3-18) into equation (3-28) yields

$$\{y\}_{total} = \{y\}_{rigid} + \sum_{i=1}^n \{\phi\}_i q_i \quad (3-29)$$

3.2.1 Development of the Mass and Stiffness Matrices of the Un-damped System

The equations of motion are derived through the use of Lagrange's equation

$$\frac{d}{dt} \left(\frac{\partial T}{\partial \dot{q}_i} \right) - \frac{\partial T}{\partial q_i} + \frac{\partial U}{\partial q_i} = Q_i \quad (3-30)$$

where T is the total kinetic energy of the system, U is the total potential energy of the system, q is a generalized coordinate and Q is a generalized force. In order to simplify the derivation, damping terms are omitted since the effects of damping do not influence the natural frequencies of the system. Damping terms are, however, important and will be addressed later in the model development. From Figure (3-1) and equation (3-29) the total kinetic and potential energy of the system are expressed as

$$\begin{aligned}
T = & \frac{1}{2} m_B \dot{y}^2 + \frac{1}{2} J_B \dot{\theta}^2 + \frac{1}{2} m_{A1} (\dot{y} + l_{A1} \dot{\theta} + \phi_{A11} \dot{q}_{A1} + \phi_{A12} \dot{q}_{A2} + \dots)^2 \\
& + \frac{1}{2} m_{A2} (\dot{y} + l_{A2} \dot{\theta} + \phi_{A21} \dot{q}_{A1} + \phi_{A22} \dot{q}_{A2} + \dots)^2 \\
& + \dots \\
& + \frac{1}{2} m_{S1} (\dot{y} + l_{S1} \dot{\theta} + \phi_{A n1} \dot{q}_{A1} + \phi_{A n2} \dot{q}_{A2} + \dots + \phi_{S11} \dot{q}_{S1} + \phi_{S12} \dot{q}_{S2} + \dots)^2 \\
& + \frac{1}{2} m_{S2} (\dot{y} + l_{S2} \dot{\theta} + \phi_{A n1} \dot{q}_{A1} + \phi_{A n2} \dot{q}_{A2} + \dots + \phi_{S21} \dot{q}_{S1} + \phi_{S22} \dot{q}_{S2} + \dots)^2 \quad (3-31) \\
& + \dots \\
& + \frac{1}{2} m_{Y1} (\dot{y} + l_{Y1} \dot{\theta} + \phi_{Y11} \dot{q}_{Y1} + \phi_{Y12} \dot{q}_{Y2} + \dots)^2 \\
& + \frac{1}{2} m_{Y2} (\dot{y} + l_{Y2} \dot{\theta} + \phi_{Y21} \dot{q}_{Y1} + \phi_{Y22} \dot{q}_{Y2} + \dots)^2 \\
& + \dots
\end{aligned}$$

$$\begin{aligned}
U = & \frac{1}{2} K_{Brg} y^2 + \frac{1}{2} K_{A1} (\phi_{A11} q_{A1} + \phi_{A12} q_{A2} + \dots)^2 \\
& + \frac{1}{2} K_{A2} ((\phi_{A21} - \phi_{A11}) q_{A1} + (\phi_{A22} - \phi_{A12}) q_{A2} + \dots)^2 \\
& + \dots \\
& + \frac{1}{2} K_{An} ((\phi_{An1} - \phi_{A(n-1)1}) q_{A1} + (\phi_{An2} - \phi_{A(n-1)2}) q_{A2} + \dots)^2 \\
& + \frac{1}{2} K_{S1} (\phi_{S11} q_{S1} + \phi_{S12} q_{S2} + \dots)^2 \\
& + \frac{1}{2} K_{S2} ((\phi_{S21} - \phi_{S11}) q_{S1} + (\phi_{S22} - \phi_{S12}) q_{S2} + \dots)^2 \\
& + \dots \\
& + \frac{1}{2} K_{Sn} ((\phi_{Sn1} - \phi_{S(n-1)1}) q_{S1} + (\phi_{Sn2} - \phi_{S(n-1)2}) q_{S2} + \dots)^2 \\
& + \frac{1}{2} K_{Y1} (\phi_{Y11} q_{Y1} + \phi_{Y12} q_{Y2} + \dots)^2 \\
& + \frac{1}{2} K_{Y2} ((\phi_{Y21} - \phi_{Y11}) q_{Y1} + (\phi_{Y22} - \phi_{Y12}) q_{Y2} + \dots)^2 \\
& + \dots \quad (3-32) \\
& + \frac{1}{2} K_{Yn} ((\phi_{Yn1} - \phi_{Y(n-1)1}) q_{Y1} + (\phi_{Yn2} - \phi_{Y(n-1)2}) q_{Y2} + \dots)^2
\end{aligned}$$

Substituting the kinetic and potential energy equations into Lagrange's equation and solving yields a set of n equations where n is number of DOF of the system. The number of flexible modes and rigid body modes that are considered determines the number of DOF of the system. Putting the equations in matrix form, as in equation (3-2), yields the following mass and stiffness matrices.

$$[M] = \begin{bmatrix} \begin{array}{c} \text{col. 1-7} \\ m_T \quad 0 \quad \Gamma_{Y1} \quad \Gamma_{Y2} \quad \cdots \quad \Gamma_{A1} + m_{ST}\phi_{An1} \quad \Gamma_{A2} + m_{ST}\phi_{An2} \\ 0 \quad J_T \quad 0 \quad 0 \quad \cdots \quad 0 \quad 0 \\ \Gamma_{Y1} \quad 0 \quad 1 \quad 0 \quad \cdots \quad 0 \quad 0 \\ \Gamma_{Y2} \quad 0 \quad 0 \quad 1 \quad \cdots \quad 0 \quad 0 \\ \vdots \quad \vdots \quad \vdots \quad \vdots \quad \ddots \quad \vdots \quad \vdots \\ \Gamma_{A1} + m_{ST}\phi_{An1} \quad 0 \quad 0 \quad 0 \quad \cdots \quad 1 + m_{ST}\phi_{An1}^2 \quad m_{ST}\phi_{An2}\phi_{An1} \\ \Gamma_{A2} + m_{ST}\phi_{An2} \quad 0 \quad 0 \quad 0 \quad \cdots \quad m_{ST}\phi_{An1}\phi_{An2} \quad 1 + m_{ST}\phi_{An2}^2 \\ \Gamma_{A3} + m_{ST}\phi_{An3} \quad 0 \quad 0 \quad 0 \quad \cdots \quad m_{ST}\phi_{An1}\phi_{An3} \quad m_{ST}\phi_{An2}\phi_{An3} \\ \vdots \quad \vdots \quad \vdots \quad \vdots \quad \ddots \quad \vdots \quad \vdots \\ \Gamma_{S1} \quad 0 \quad 0 \quad 0 \quad \cdots \quad \Gamma_{S1}\phi_{An1} \quad \Gamma_{S1}\phi_{An2} \\ \Gamma_{S2} \quad 0 \quad 0 \quad 0 \quad \cdots \quad \Gamma_{S2}\phi_{An1} \quad \Gamma_{S2}\phi_{An2} \\ \vdots \quad \vdots \quad \vdots \quad \vdots \quad \ddots \quad \vdots \quad \vdots \end{array} \\ \begin{array}{c} \text{col. 8-12} \\ \Gamma_{A3} + m_{ST}\phi_{An3} \quad \cdots \quad \Gamma_{S1} \quad \Gamma_{S2} \quad \cdots \\ 0 \quad \cdots \quad 0 \quad 0 \quad \cdots \\ 0 \quad \cdots \quad 0 \quad 0 \quad \cdots \\ 0 \quad \cdots \quad 0 \quad 0 \quad \cdots \\ \vdots \quad \vdots \quad \vdots \quad \vdots \quad \ddots \\ m_{ST}\phi_{An3}\phi_{An1} \quad \cdots \quad \Gamma_{S1}\phi_{An1} \quad \Gamma_{S2}\phi_{An1} \quad \cdots \\ m_{ST}\phi_{An3}\phi_{An2} \quad \cdots \quad \Gamma_{S1}\phi_{An2} \quad \Gamma_{S2}\phi_{An2} \quad \cdots \\ 1 + m_{ST}\phi_{An3}^2 \quad \cdots \quad \Gamma_{S1}\phi_{An3} \quad \Gamma_{S2}\phi_{An3} \quad \cdots \\ \vdots \quad \ddots \quad \vdots \quad \vdots \quad \ddots \\ \Gamma_{S1}\phi_{An3} \quad \cdots \quad 1 \quad 0 \quad \cdots \\ \Gamma_{S2}\phi_{An3} \quad \cdots \quad 0 \quad 1 \quad \cdots \\ \vdots \quad \vdots \quad \vdots \quad \vdots \quad \ddots \end{array} \end{bmatrix} \quad (3-33)$$

$$[K] = \begin{bmatrix} K_{bearing} & 0 & 0 & 0 & 0 & 0 & 0 & 0 & 0 & 0 & 0 & 0 \\ 0 & 0 & 0 & 0 & 0 & 0 & 0 & 0 & 0 & 0 & 0 & 0 \\ 0 & 0 & \omega_{y1}^2 & 0 & 0 & 0 & 0 & 0 & 0 & 0 & 0 & 0 \\ 0 & 0 & 0 & \omega_{y2}^2 & 0 & 0 & 0 & 0 & 0 & 0 & 0 & 0 \\ 0 & 0 & 0 & 0 & \ddots & 0 & 0 & 0 & 0 & 0 & 0 & 0 \\ 0 & 0 & 0 & 0 & 0 & \omega_{A1}^2 & 0 & 0 & 0 & 0 & 0 & 0 \\ 0 & 0 & 0 & 0 & 0 & 0 & \omega_{A2}^2 & 0 & 0 & 0 & 0 & 0 \\ 0 & 0 & 0 & 0 & 0 & 0 & 0 & \omega_{A3}^2 & 0 & 0 & 0 & 0 \\ 0 & 0 & 0 & 0 & 0 & 0 & 0 & 0 & \ddots & 0 & 0 & 0 \\ 0 & 0 & 0 & 0 & 0 & 0 & 0 & 0 & 0 & \omega_{S1}^2 & 0 & 0 \\ 0 & 0 & 0 & 0 & 0 & 0 & 0 & 0 & 0 & 0 & \omega_{S2}^2 & 0 \\ 0 & 0 & 0 & 0 & 0 & 0 & 0 & 0 & 0 & 0 & 0 & \ddots \end{bmatrix} \quad (3-34)$$

where

$$\{y\} = \begin{Bmatrix} y \\ \theta \\ q_{y1} \\ q_{y2} \\ \vdots \\ q_{A1} \\ q_{A2} \\ q_{A3} \\ \vdots \\ q_{S1} \\ q_{S2} \\ \vdots \end{Bmatrix} \quad (3-35)$$

In the derivation of the system equations, the identities established below were utilized, in conjunction with the identities established in equations (3-14), (3-15), (3-16), (3-17), and (3-27), to simplify the mass and stiffness matrices.

$$m_{ST} = \sum_{i=1}^n m_{Si} \quad (3-36)$$

The total mass of the suspension sub-component FE model is represented by m_{ST} , and each lumped nodal mass is represented by m_{Si} .

$$m_T = m_B + \sum_{i=1}^{n_y} m_{y_i} + \sum_{j=1}^{n_A} m_{A_j} + \sum_{k=1}^{n_s} m_{S_k} \quad (3-37)$$

The total mass of the HSA is represented by m_T . The mass of the rigid body (as shown in Figure (3-1)) is represented by m_B . As in equation (3-36), the mass of the yoke/coil, arm, and suspension sub-component FE models are represented by the Σm terms.

$$J_T = J_B + \sum_{i=1}^{n_y} m_{y_i} l_{y_i}^2 + \sum_{j=1}^{n_A} m_{A_j} l_{A_j}^2 + \sum_{k=1}^{n_s} m_{S_k} l_{S_k}^2 \quad (3-38)$$

The total mass moment of inertia of the HSA about the pivot center is represented by J_T . The mass moment of inertia of the rigid body about the pivot center is represented by J_B . The mass moment of inertia of the yoke/coil, arm, and suspension sub-component FE models about the pivot center are represented by the Σml^2 terms.

3.2.2 Development of the Force Input Vector

From Figure (3-1) and equation (3-24) the input force vector can be shown to be

$$\{F\} = \begin{Bmatrix} F_o \\ F_o R_c \\ \phi_{Y11} F_o \\ \phi_{Y12} F_o \\ \vdots \\ 0 \\ 0 \\ 0 \\ \vdots \\ 0 \\ 0 \\ \vdots \end{Bmatrix} \quad (3-39)$$

where R_c represents the moment arm from the HSA pivot center to the force applied by the coil. The HSA is moved and positioned by a voice coil motor (VCM) which consists of a coil of wire (as shown in Figure (1-1)) “sandwiched” between two magnets.

Applying a current I through the coil induces a torque T on the HSA which causes an angular acceleration. The magnitude of the torque is proportional to the product of the current I and torque constant K_t of the VCM.

$$T = K_t I \quad (3-40)$$

The units of K_t are usually expressed in oz-in/Amp. Since the forces that move and position the HSA are generated by applying current to the VCM, the input forces in the y and θ directions of equation (3-39) can be re-written in terms of the torque constant and input current as

$$F_o = \frac{K_t}{R_c} I \quad (3-41)$$

and

$$F_o R_c = K_t I \quad (3-42)$$

The force generated by current flow through a constant magnetic field is the vector cross product of the vector representing the direction of the current flow and the vector representing the direction of the magnetic flux density. Due to the orientation of the coil in the magnetic field, only the sides, or the active lengths, of the coil are useful for generating torque to move the HSA (as shown in Figure (3-2)). The force vectors

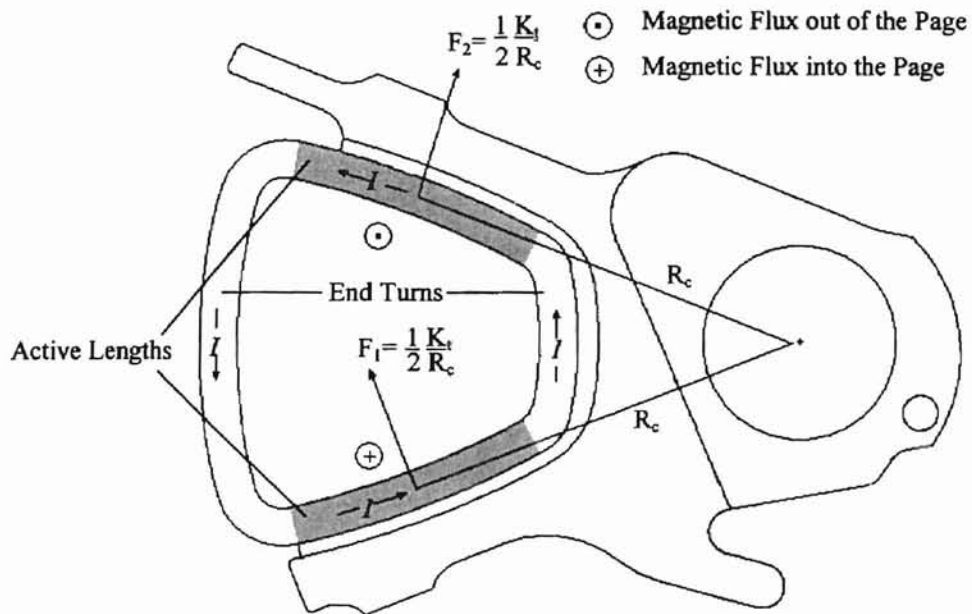


Figure 3-2: Forces due to Current Input to the Coil

generated by the ends of the coil, or end turns, are directed either towards or away from the pivot center and provide little or no torque. Typically, only the active lengths of the coil are exposed to the magnetic field. Each active length provides one-half of the force and therefore one-half of the torque generated when current is passed through the coil. The force is assumed to be uniformly distributed along the active length of the coil and can be approximated as a single force vector acting at the center of the active length, as

illustrated in Figure (3-2). The moment arm, R_c , is therefore the distance from the pivot center to the center of an active length.

Since the input force to the HSA model can be approximated as two equal forces, each force is assumed to act at a single node at the mid-point of each active length in the yoke/coil sub-component FE model. From equation (3-24), for each yoke mode considered, the mode shape values (ϕ) for the two nodes where the forces are assumed to act, must be known, and can be obtained from the yoke/coil sub-component FE model. Thus, the input force from equation (3-39) can be re-written as

$$\phi_{Y1} F_o = (\phi_{Yj1_{F1}} + \phi_{Yk1_{F2}}) \frac{1}{2} \frac{K_t}{R_c} \quad (3-43)$$

Substituting equations (3-41), (3-42), and (3-43) into equation (3-39) yields the force input vector in terms of the input current.

$$\{F\} = \left\{ \begin{array}{c} \frac{K_t}{R_c} \\ K_t \\ (\phi_{Yj1_{F1}} + \phi_{Yk1_{F2}}) \frac{1}{2} \frac{K_t}{R_c} \\ (\phi_{Yj2_{F1}} + \phi_{Yk2_{F2}}) \frac{1}{2} \frac{K_t}{R_c} \\ \vdots \\ 0 \\ 0 \\ 0 \\ \vdots \\ 0 \\ 0 \\ \vdots \end{array} \right\} I \quad (3-44)$$

3.2.3 HSA Modeling Assumptions

During the development of the HSA model, several assumptions were made in order to simplify the equation derivations and the resulting mass and stiffness matrices. First, as previously mentioned, damping was omitted. The resonances of the HSA are typically lightly damped and minimally coupled to adjacent modes so that damping does not effect the calculation of the natural frequencies of the individual resonances. The primary influence of damping in the HSA model is that of limiting the amplitude response at resonance. Since damping limits the amplitude at resonance, damping will be accounted for later in the model development in order for the HSA model to accurately predict off-track motion during track following. When damping is added, damping terms will be treated as viscous, or proportional, damping.

Second, the HSA model is limited to track following. By limiting the model to track following as opposed to seeking, the HSA can be assumed to behave as a linear system. During seeking, the input current to the coil, and therefore the forces acting on the HSA, is significantly greater compared to the input current and resulting forces that act on the HSA during track following. The increased forces applied on the HSA and the frequency content of a seek profile, can excite non-linear resonances that otherwise would not be excited. Also during seeking, modes that were previously considered linear may begin to exhibit non-linear behavior.

During track following, there is very little rotation of the HSA. By limiting the model to track following, the angular accelerations, velocities, and displacements of the HSA are limited to small values such that the coupling between the rotational DOF (θ) and the modal (q_{Yi}, q_{Ai}, q_{Si}) DOF can be assumed negligible. This is an important

assumption since the coupling factors between the rotational and modal DOF are difficult to calculate. The modal participation factors (Γ) and mode shape values (ϕ) used to couple the translational (y) and modal (q_{Yi}, q_{Ai}, q_{Si}) DOF in the mass matrix are obtained from the sub-component FE normal mode solution. The modal participation factors and mode shape values are typically made available as outputs of the FE software. The rotational to modal coupling factors that are obtained through the derivation of the system equations are of the form

$$rmcf_j = \sum_{i=1}^n m_i \phi_{ij} l_i \quad (3-45)$$

where $rmcf_j$ is the rotational to modal coupling factor for the j^{th} mode, m_i is the i^{th} lumped nodal mass, ϕ_{ij} is the correspond mode shape value, and l_i is the corresponding moment arm from the pivot center to the i^{th} nodal mass. In order to calculate the rotational to modal coupling factors, a custom solver would have to be developed and used to solve the sub-component FE models. The validity of the assumption that the rotational to modal coupling factor is zero may be tested by placing terms in the mass matrix that couple the rotational and modal DOF (the artificial coupling terms must be of the same order of magnitude as other terms in the matrix). Re-solving the system equations shows that the addition of the coupling terms does not alter the frequency response of the system. The conclusion can therefore be drawn that the assumption previously discussed is valid.

Lastly, the HSA is assumed to be perfectly balanced so that the center of gravity is at the pivot center. This assumption removes any coupling terms between the translational (y) and rotational (θ) DOF. Imbalance of the HSA is primarily a concern for

external shock and vibration disturbance inputs. In the case of external disturbances, any amount of imbalance in the HSA can be detrimental to the overall drive performance. Thus drive design engineers strive to minimize imbalance in the HSA. Realistically, because of manufacturing tolerances, the center of gravity is always offset from the pivot center so that every HSA has some amount of imbalance. Even though imbalance terms are not included, the effects of imbalance can easily be studied with the HSA model that has been derived. Imbalance terms can be calculated and placed in the mass matrix to couple the translational and rotational DOF. However, just as the rotational to nodal coupling terms do not effect the modeled frequency response, the rotational to translational coupling terms will have almost no effect on the track following frequency response of the model.

3.2.4 HSA Model Discussion

In the model development, the mechanical resonances of the HSA have been divided into flexible and rigid body modes. The flexible resonances, as calculated utilizing the sub-component FE models, result from the material properties and boundary conditions of each sub-component system. The rigid body modes result from the moving mass and rotational inertia of the HSA. Specifically, the two rigid body modes considered in the model are the modes relating to and resulting from the translation and rotation of the HSA in the y and θ coordinate systems.

Since the HSA is free to rotate about the pivot bearings, the rigid body rotational mode is an unconstrained mode at 0 Hz. The rigid body translational mode, or bearing translational mode, is actually, in all technical accuracy, not a true rigid body mode since

it is dependent on the deformation of the pivot bearings. Also, at the frequency that the rigid body translational mode occurs, the sub-components may deform. However, it is referred to as a rigid mode in this paper as it primarily results from the moving mass of the HSA and the spring constants of the pivot bearings. The natural frequency of the rigid body translation mode can be approximated by

$$\omega_{Translation} = \sqrt{\frac{K_{bearing}}{M_T}} \quad (3-46)$$

The resulting HSA model is an n -DOF model where n is the total number of modes considered. The model consists of two rigid body modes, as previously mentioned, and $n-2$ flexible modes of the yoke/coil, suspension, and arm. Each flexible mode is considered as a single-DOF system in a modal coordinate system q_i . The system equations are dynamically coupled through the mass matrix. The coupling terms in the mass matrix are comprised of the modal participation factors (Γ) and specific mode shape values (ϕ) obtained from the arm sub-component FE model. These coupling factors indicate how the flexible sub-component and rigid body modes interact to form the overall system dynamics. In the presence of support or ground motion, the modal participation factor describes to what extent a given mode is excited. For the forced vibration case, the modal participation factor describes to what extent the excited mode transmits the input force to the ground or support structure.

The HSA model does not require that all mode shape values associated with each node in the sub-component FE model be extracted. For each sub-component mode considered, only the mode shape values at nodes where displacements of the FE model must be known (such as the arm tip and slider) and nodes where forces are assumed to

act are extracted from the sub-component model. This limits the number mode shape values that must be obtained from the FE model to one or two values per mode for each sub-component.

For each yoke mode considered, only the two mode shape values associated with the nodes where the input force is assumed to act are required. These mode shape values are used in the force input equation (equation (3-44)). For each arm mode considered, only one mode shape value at the tip of the arm where the suspension is attached is required. The arm mode shape value describes the displacement due to deformation of the arm tip. This arm mode shape value is the only modal value (ϕ_{Ani}) that shows up in the mass matrix (equation (3-33)). It is part of the coupling factor between the arm and suspension since the total displacement of the base of the suspension is the sum of the rigid body motion and the deformation displacement of the arm tip. Likewise, for the suspension FE model, only one mode shape value per mode is required. The mode shape that is required from the suspension FE model is a modal value on the slider since it is ultimately the displacement of the slider that is detrimental to the drive performance. The mode shape value extracted from the suspension FE model is used only in the output equation shown below (equation (3-53)).

The FE software used in this thesis was Structural Dynamics Research Corporation (SDRC) Ideas Master Series 7. SDRC calculates the modal participation factor as part of an effective mass term. SDRC defines the effective mass as

$$M_{e_i} = \frac{\Gamma_i^2}{mm_i m_T} \quad (3-47)$$

where M_e is the effective mass, Γ is the modal participation factor, mm is the modal mass, m_T is the total mass of the FE modal and i denotes the mode number. The modal participation factor can be calculated by rearranging terms.

$$\Gamma_i = \sqrt{M_e mm_i m_T} \quad (3-48)$$

3.2.5 State Space Representation of the HSA Model

For simulation purposes, the equations are recast in a state space representation where the system equations are described by a set of first order differential equations. In state space form, the state of the system at any given time can be described by the displacement and velocity of the system, which are called state variables. The state space matrix equations take the general form given below

$$\{\dot{x}\} = [A]\{x\} + [B]u \quad (3-49)$$

where $[A]$ is the system matrix, $[B]$ is the input matrix, and $\{x\}$ is the state variable vector. The output equation can also be expressed in matrix form as

$$\{y\} = [C]\{x\} + [D]u \quad (3-50)$$

where $[C]$ is the output matrix and $[D]$ is the direct transmission matrix. Expressing equation (3-1) in state space form yields the following

$$\begin{Bmatrix} \dot{y} \\ \ddot{y} \end{Bmatrix} = \underbrace{\begin{bmatrix} 0 & I \\ -[M]^{-1}[K] & -[M]^{-1}[C_{damp}] \end{bmatrix}}_{[A]} \begin{Bmatrix} y \\ \dot{y} \end{Bmatrix} + \underbrace{\begin{bmatrix} 0 \\ [M]^{-1}\{F\} \end{bmatrix}}_{[B]} u \quad (3-51)$$

where $[M]$ and $[K]$ are the mass and stiffness matrices and $\{F\}$ is the input force vector. For the HSA model, the input term u represents the coil input current I from equation (3-44).

In equation (3-51), the term $[M]^{-1}[C_{damp}]$ represents the damping of the system. Damping terms were previously ignored in the model development. For the HSA model, proportional damping is assumed so that the resulting damping matrix is diagonal.

$$[M]^{-1}[C_{damp}] = \text{diag}[2\xi\omega_i] \quad (3-52)$$

For the HSA model, the output and direct transmission matrices $[C]$ and $[D]$ are

$$[C] = [1 \quad -R_h \quad 0 \quad 0 \quad \dots \quad 0 \quad 0 \quad 0 \quad \dots \quad \phi_{Sn1} \quad \phi_{Sn2} \quad \dots]$$

and (3-53)

$$[D] = 0$$

where R_h is the distance from the pivot center to the slider. The output matrix $[C]$ is the modal superposition of the rigid body and flexible modes that directly contribute to the off-track displacement of the slider.

4 Finite-Element Models

4.1 Full HSA Finite-Element Model

To illustrate the difficulties in dealing with large FE models of complex structures, a full FE model of the HSA will first be presented. The results of the full HSA model were not used in the development of the sub-component FE analytical model. Figure 4-1

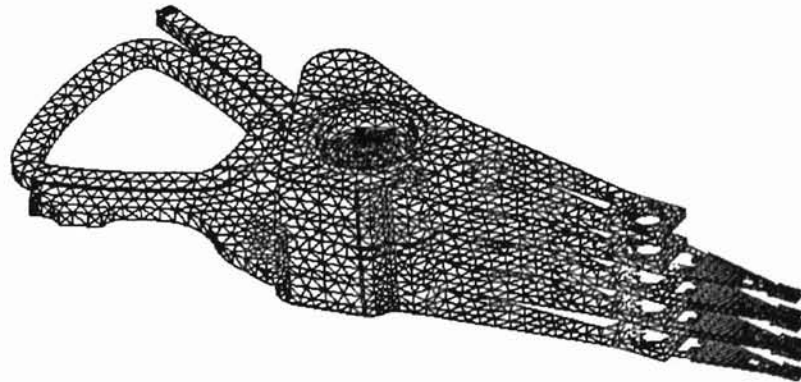


Figure 4-1: Full HSA FE Model

shows the full FE model of a typical HSA. The FE software used for all FE models presented in this paper is SDRC Ideas Master Series 7 running on a Windows NT platform. The HSA FE model consists of the actuator, coil, pivot bearings, and six suspensions. The actuator and coil are composed of solid tetrahedral elements with

mid-side nodes. Each suspension is comprised mainly of thin shell elements with the exception of the sliders, which were meshed using solid brick elements. The pivot bearings were modeled as sixteen linear springs connected between the actuator and bearing shaft. The total number of elements for the full HSA model is approximately 22,000 and the total number of nodes is approximately 39,000. The boundary conditions of the HSA model are such that the actuator is clamped at the top and bottom of the bearing shaft and the six sliders are constrained to move only in the off-track direction. The model development time for the full HSA FE model was approximately 80 hours. All mode shapes and frequencies for the HSA under 17 kHz, approximately 80 modes, were calculated. Due to the size of the model, the solve time was over 12 hours for a single processor Pentium II 350 system with 256 MB of memory. The calculated natural frequencies of the HSA are generally within 10% of experimental data, although the mode shape amplitudes do not correspond quite as well. The discrepancies between the FE HSA model and measured data can be seen in Figure 4-2. Figure 4-2 compares the mechanical frequency response of the FE model due to a harmonic input at the coil and a displacement output at the slider to the measured frequency response from a hard disk drive. The discrepancies between the measured and modeled transfer function are due to errors in the FE model. Possible sources of error include improperly modeled pivot bearings, improperly modeled coil (including inaccurate assumptions regarding coil material properties), improperly modeled interface between the actuator and bearings, improper boundary conditions (either too rigid or too soft), and the fact that the center of gravity of the FE model is offset from the pivot center. All of the errors in the FE model that contribute to the discrepancies between the measured and modeled transfer

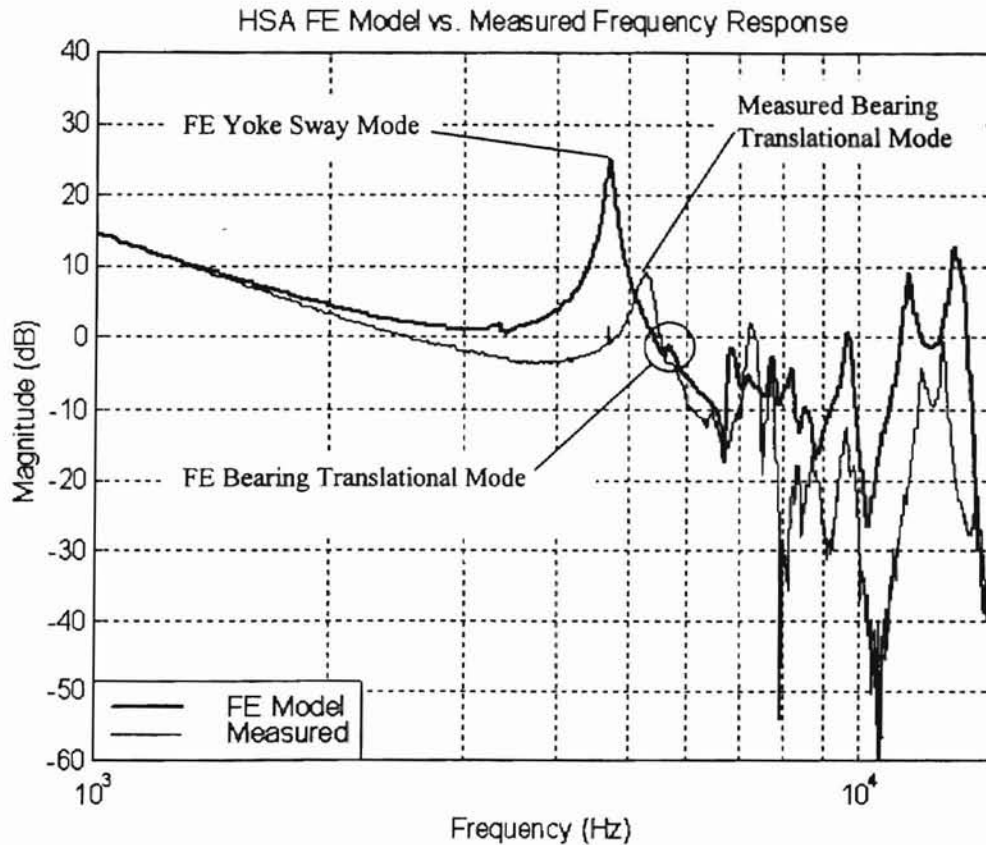


Figure 4-2: HSA FE Model vs. Measured Mechanical Transfer Function

functions can be corrected so that the modeled results agree more closely with the measured data. However, due to the size of the model and the required solve time, determining the exact cause of the errors and correcting the FE model would be extremely time consuming. Thus the full FE model should not be used to produce theoretical transfer functions.

4.2 Sub-Component FE Models

Because of the complexity of the full HSA FE model, the HSA can be broken into three sub-component FE models. The three smaller FE models consist of the coil and yoke, a single arm with two suspensions, and a single suspension. These three models are much smaller than the full model and take only minutes, compared to hours, to solve.

The smaller sub-component models can be solved in system memory where as the full model requires the use of virtual memory. Virtual memory requires dumping the system memory to the hard drive and reading it back at a later time when the information is needed. Any time a solution requires the use of virtual memory, the solve time increases dramatically.

The boundary conditions of the sub-component models are critical if these models are to agree with measured data. To verify the boundary condition assumptions as well as the accuracy of each sub-component FE model, the calculated natural frequencies and mode shapes are compared against measured data. Typically, the calculated natural frequency for each mode shape is within 7% of experimental data. Even though each FE model represents only a sub-component of the total HSA, all experimental data is measured from full HSAs in working drives. The sub-component FE models are compared to full HSAs since the purpose of the sub-component model is to reduce the complexity associated with creating and solving FE models of complex structures while retaining accurate prediction capabilities for the natural frequencies and mode shapes of the various HSA components. Thus, even though the sub-component FE models represent only a portion of the entire HSA, the associated FE model should be able to accurately predict the natural frequencies and corresponding mode shapes as if each sub-component FE model were part of a complete HSA.

4.2.1 Suspension FE Model

Figure 4-3 shows a typical model of a suspension. The model consists of approximately 360 elements and approximately 490 nodes. The suspension is modeled using predominately thin shell elements, the exception being the slider, which is meshed

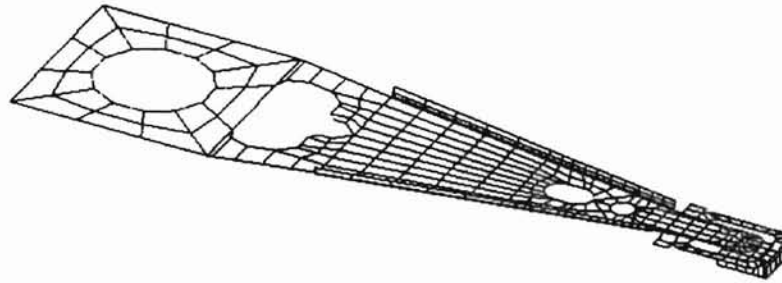


Figure 4-3: Suspension Sub-Component FE Model

using solid brick elements. The nodes of the suspension around the swage hole, or base of the suspension, are constrained in all six degrees of freedom and the four corners of the slider are constrained with zero displacement in the vertical or z-axis. The slider is free to move side to side or front to back. This constraint on the slider accurately models the air bearing, the thin layer of air that separates the slider from the disk under operating conditions, which has an axial stiffness of greater than 30 kHz. The justification for the rigidly clamped boundary conditions around the swage hole is based on the assumption that the flexibility of the arm does not significantly affect the mode shape of the suspension. This is a valid assumption since drive design engineers strive to minimize coupling not only between the arm and suspensions but also between any components in the disk drive. If coupling exists, the track following performance of the disk drive is degraded since coupled or adjacent modes without sufficient frequency separation can cause greater displacements of the slider than individual modes. The model development time for the suspension model was approximately 5 hours and the solve

time on a Pentium II 350 system with 256 MB of memory was less than 1 min. Table 4-1 shows the results of the single suspension FE model compared with measured data. The suspension mode shapes calculated from the sub-component FE model are shown in Appendix A.

Mode Shape	Modeled Frequency (kHz)	Measured Frequency (kHz)	% Difference
1 st Bending	1.87	1.97	-5.1
1 st Torsion	4.05	3.68	10.1
2 nd Bending	5.82	5.61	3.7
2 nd Torsion	10.66	9.88	7.9
3 rd Bending	11.77	11.80	-0.3

Table 4-1: Suspension FE Model vs. Measured Natural Frequencies

4.2.2 Actuator Arm FE Model

The second sub-component model is of the actuator arm as seen in figure 4-4. The

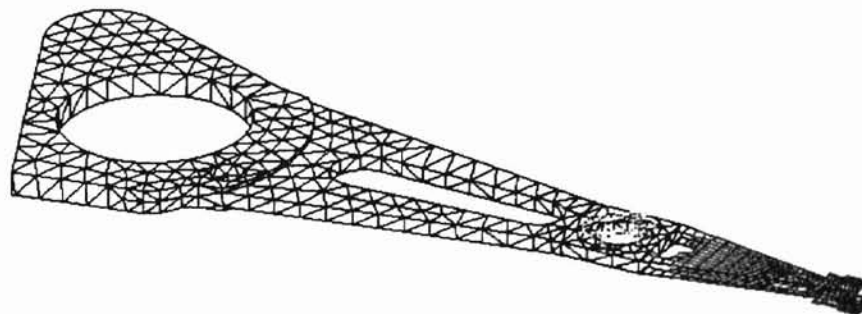


Figure 4-4: Actuator Arm Sub-Component FE Model

model consists of approximately 2150 elements and approximately 4000 nodes. The arm model consists of a single actuator arm and two suspensions and is meshed with solid tetrahedral elements with mid-side nodes (the suspensions are as described above). For the arm, the nodes at the base of the arm that form the body of the actuator are constrained in all six degrees of freedom to model the arm being rigidly clamped. The two suspensions are joined to the arm model by merging coincident nodes on both the arm and suspensions so that the suspensions are rigidly attached to the arm. The boundary conditions for the sliders are the same as for the single suspension model. For the FE model of the sub-components to be accurate, the boundary conditions must be correct. Thus it is necessary to include the two suspensions in the arm model. The suspensions provide mass and inertia that dramatically affect the mode shapes and frequencies of the arm. It appears redundant to solve FE models of the arm with two suspensions as well as a separate model of a single suspension since the arm model solution will give the natural frequencies and mode shapes for the both the arm and suspensions. However, there are two advantages in treating the suspension and arm as separate sub-components in the model development. First, by treating the two as separate sub-components, the coupling factors between the arm and suspension modes can be calculated, lending understanding as to how the suspension is excited by the arm and how the arm is excited by the suspension. Second, once the model is developed, new suspension designs can be evaluated quickly without the creation of a new arm model. The suspension model must be created first anyway. The model development time for the arm model was approximately 1 hour (the suspension model is assumed to already exist) and the solve time on a Pentium II 350 system with 256 MB of memory

was less than 3 min. Table 4-2 shows the results of the arm FE model compared with measured data. The arm mode shapes calculated from the sub-component FE model are shown in Appendix B.

Mode Shape	Modeled Frequency (kHz)	Measured Frequency (kHz)	% Difference
1 st Bending	1.08	1.14	-5.3
2 nd Bending	7.51	7.69	-2.3
1 st Torsion	7.73	7.79	-0.8

Table 4-2: Actuator Arm FE Model vs. Measured Natural Frequencies

4.2.3 Yoke and Coil FE Model

The third sub-component model is of the yoke and coil as seen in Figure 4-5. The model

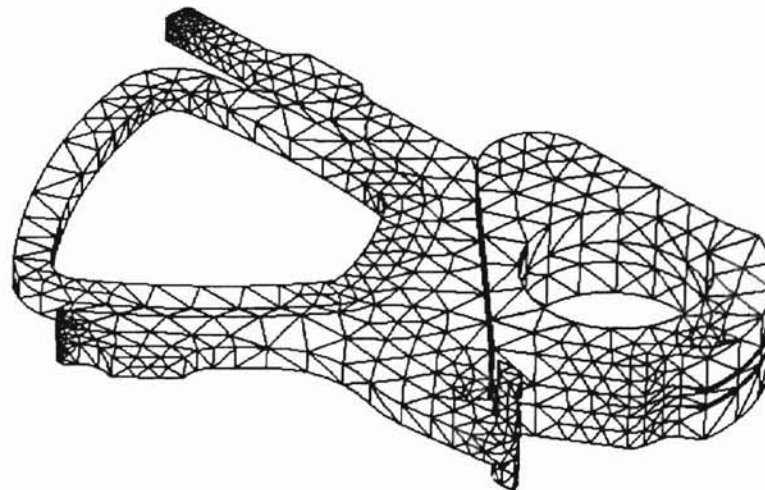


Figure 4-5: Yoke/Coil Sub-Component FE Model

consists of approximately 2600 elements and 5100 nodes. The yoke/coil model consists of three parts: the yoke, the coil, and the epoxy that bonds the coil to the yoke. All

elements used in the yoke/coil model are solid tetrahedral elements with mid-side nodes. Similar to the arm model, the nodes at the base of the yoke that form the body of the actuator are constrained in all six degrees of freedom to model the yoke being clamped rigidly. Since the coil is not solid, the material properties (Young's modulus and mass density) are difficult to determine. The density value that is used in the FE model is adjusted so that FE model of the coil has the correct weight for the modeled coil volume. The correct Young's modulus is found by iterating until the frequencies of the first few modes agree with measured data. Since the model of the yoke/coil is small, the iteration process only takes a few minutes. Once the Young's modulus is found, this value can be used in future yoke models that contain similar coil designs. The epoxy that bonds the coil to the yoke provides no structural stiffness to the system. The Young's modulus that is used for the epoxy is simply several orders of magnitude less than that of aluminum, the material of the yoke. Often the coil is modeled as an orthotropic material, but this step is not necessary to accurately predict the frequency and mode shapes for the first few modes. The model development time for the yoke/coil model was approximately 2 hours and the solve time on a Pentium II 350 system with 256 MB of memory was less than 5min. Table 4-3 shows the results of the yoke/coil FE model compared with measured data. The yoke/coil mode shapes calculated from the sub-component FE model are shown in Appendix C.

Mode Shape	Modeled Frequency (kHz)	Measured Frequency (kHz)	% Difference
1 st Bending	1.12	1.19	-5.5
1 st Torsion	1.82	1.90	-4.2

Table 4-3: Yoke/Coil FE Model vs. Measured Natural Frequencies

4.3 Experimental Verification of FE Models

Measurements of the natural frequencies and corresponding mode shapes of the suspension, actuator arm, and yoke/coil were made with a Scanning Laser Doppler Vibrometer (LDV). The LDV is an optical instrument that provides a non-contact means to measure the velocity and displacement vibrations of a surface. It is important that a non-contact technique be used since the components that are being measured are relatively small with little mass. Devices such as accelerometers can mass load the component and significantly alter the measurements. Mass loading occurs when the mass of the measurement device is a significant portion of the effective mass of a particular mode.

The scanning LDV automatically measures a set of user pre-defined points on the structure and calculates the frequency response function for each measured point. The frequency response function at each measurement point is calculated by dividing the measurement output response by the input excitation for the system. For the scanning LDV measurements of the HSA, the measurement output is the LDV vibration measurement (typically velocity) and the input excitation is a random noise current input to the coil. Once all of the points are scanned, animations of the structure can be viewed for any frequency in the measurement range since the magnitude and phase of each measurement point are known from the frequency response functions. The animations provided by the scanning LDV software are actually operating deflection shapes (ODS) not mode shapes, since no modal parameters are calculated. However, ODS are typically an accurate approximation of the mode shapes and un-damped natural frequencies of a system provided adjacent modes are not closely coupled. The scanning

LDV eliminates the tediousness and saves hours over manual data collection techniques associated with modal analysis methods.

In order to animate an ODS, numerous points on the surface of the structure to be analyzed must be measured. Since the components of the HSA are small in size, measurements with the scanning LDV are typically limited to axial (perpendicular to the disk plane) measurements to ensure a sufficient surface area for proper animation and mode shape identification. As a result, only modes that have displacement components perpendicular to the disk plane can be measured. This includes bending and torsional modes of the HSA sub-components. Modes that have deformation predominately in the plane of the disk, such as arm sway modes, are very difficult to accurately measure with the scanning LDV. Thus, in the previous tables which compare calculated and measured natural frequencies of the sub-components, sway modes are excluded. However, since the bending and torsion modes are typically within 7% of measured values, it will be assumed that the natural frequencies of the yoke, arm, and suspension sway modes are also be within 7% of the actual natural frequency.

5 HSA Model Simulation Results and Discussion

5.1 Reduced Order Model Simulation

The results of the frequency response simulation of a reduced order model will first be discussed. This model simplifies the overall dynamics of the HSA by removing the flexible modes of the sub-components. The purpose of this section is to discuss a deviation between the state-space model and measured data and show how the full order model will be compensated to correct for modeling inaccuracies. Considering only the rigid body rotational mode and the bearing translational mode reduces the model to a set of two un-coupled system equations

$$\begin{bmatrix} m_T & 0 \\ 0 & J_T \end{bmatrix} \begin{Bmatrix} \ddot{y} \\ \ddot{\theta} \end{Bmatrix} + \begin{bmatrix} K_{bearing} & 0 \\ 0 & 0 \end{bmatrix} \begin{Bmatrix} y \\ \theta \end{Bmatrix} = \begin{Bmatrix} K_i / R_c \\ K_i \end{Bmatrix} I \quad (5-1)$$

where the total displacement of the slider is

$$y_{total} = y + R_{head} \theta \quad (5-2)$$

In Figure 5-1 below, the frequency response of the reduced order model is compared with measured data from a hard disk drive. From Figure 5-1, it can be seen that the modeled system transfer function deviates from the measured data. The modeled frequency response starts to diverge from the measured frequency response at approximately 2 kHz and the modeled bearing translational mode at 5.4 kHz has a

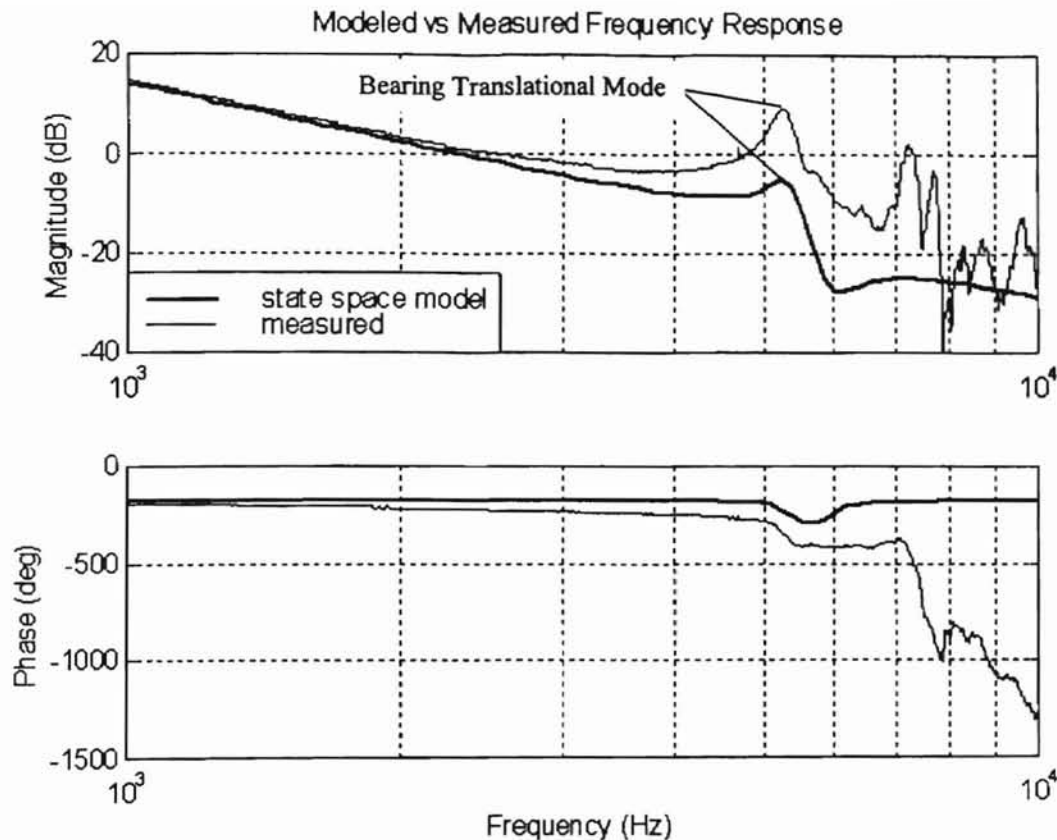


Figure 5-1: Rigid Body State Space Model vs. Measured Frequency Response

different amplitude and phase compared to the measured data. Since the output of the state space model is the sum of the translational and rotational displacements (equation (5-2)), the relationship of the two equations is critical to the overall shape of the total displacement frequency response. This is illustrated in Figure 5-2 where the individual translational and rotational components are shown. The differences between the modeled and measured frequency response functions are due the frequency at which the mass line of the rotational transfer function and the stiffness line of the translational transfer function intersect. The DC gain of each transfer function determines where the two curves intersect. For the rotational component, the DC gain is

$$K_{\theta} = \frac{K_t R_h}{J_T} K_{BW} \quad (5-3)$$

and for the translational component, the DC gain is

$$K_{Trans} = \frac{F_o}{K_{bearing}} K_{BW} = \frac{K_t}{R_c K_{bearing}} K_{BW} \quad (5-4)$$

where K_{BW} is the gain factor associated with the drive electronics and compensator. The

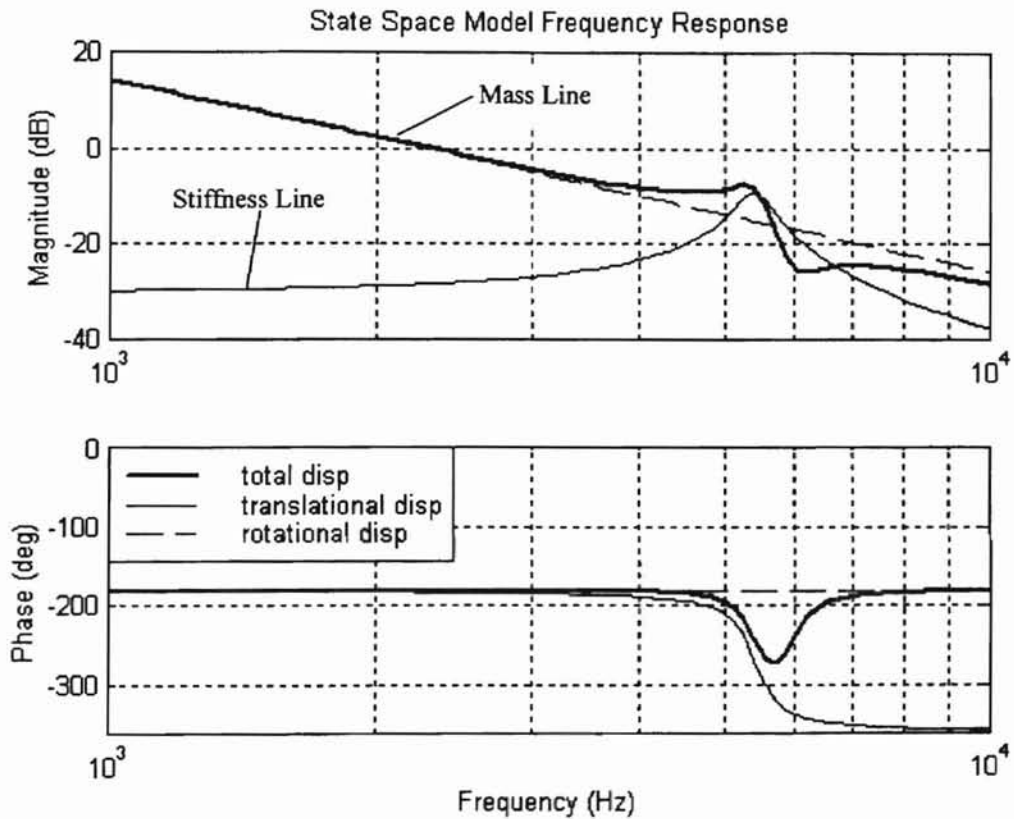


Figure 5-2: Translational and Rotational Components of the State Space Model

terms that comprise the rotational and translational DC gain terms are measurable properties of the system (torque constant (K_t), rotational inertia (J_T), bearing stiffness ($K_{bearing}$), moment arm from input force to pivot center (R_c), and moment arm from slider to pivot center (R_h)). In order for the sum of the translational and rotational equations to intersect and form a smooth transition, either the DC gain of the rotational component must be lowered or the DC gain of the bearing translational mode must be increased to

achieve the correct frequency response function. However, since the measured and modeled frequency responses do not diverge until 2 kHz, it appears that the gain for the rotational component is correct and the gain for the bearing translational mode is incorrect. Since the DC gain for the translational mode is proportional to the input force (equation (5-4)), the input force is increased until the state space model matches the measured data. The resulting gain adjustment needed to correct the error in the state space model is

$$K_{\text{adjustment}} = \frac{M_T R_h}{J_T} \quad (5-5)$$

where M_T is the total mass of the actuator, R_h is the moment arm from the pivot center to

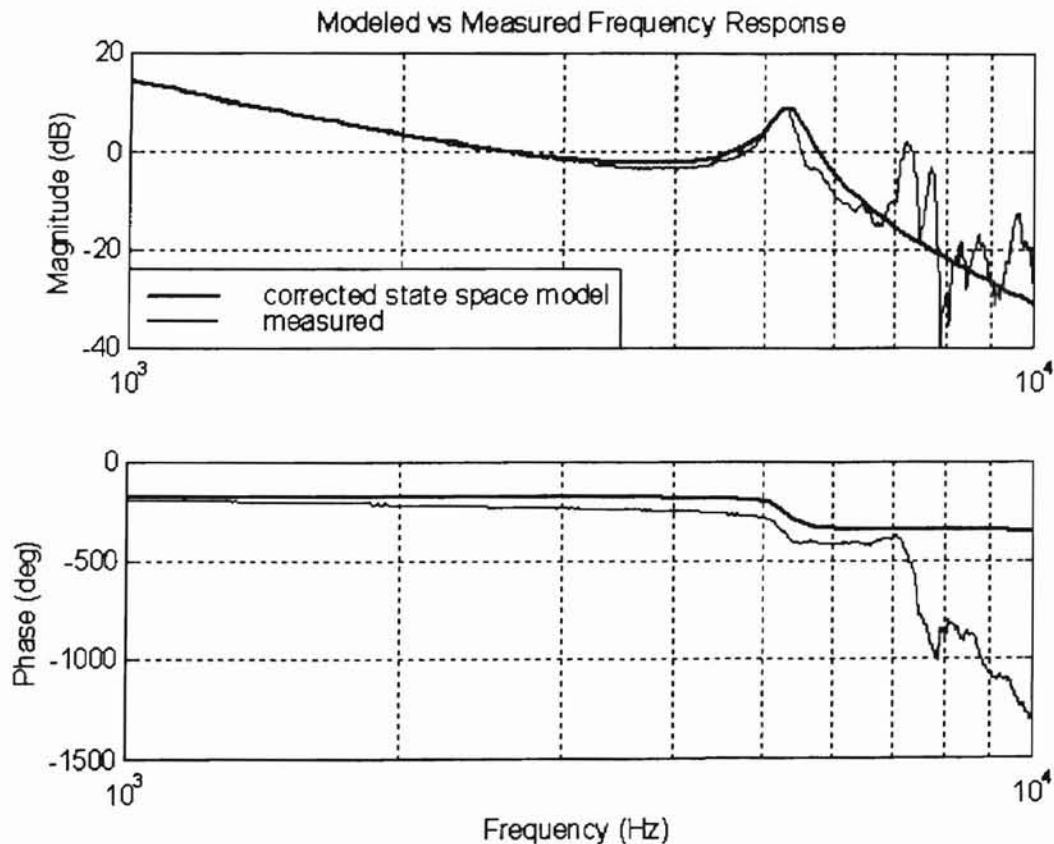


Figure 5-3: Corrected State Space Model vs. Measured Frequency Response

the slider, and J_T is the total mass moment of inertia of the HSA about the pivot center. The physical reason why the adjustment gain is needed is not fully understood at this time. However the gain adjustment term derived above is valid for all cases, not just the model presented in this paper. Applying the gain adjustment factor to the force input for the translational DOF corrects the offset problem as is seen in Figure (5-3).

In Figures 5-1 and 5-3 there is a slight difference between the calculated and measured phase below 4 kHz. From 1 kHz to 4 kHz, the measured phase decreases as frequency increases, where as the modeled phase remains constant. This phase divergence is a result of the measurement technique that was used to obtain the frequency response function from the drive. Referring to Figure 1-2, the structural response of the drive is defined as the head position divided by coil current. Both the head position and input current to the coil can be measured directly from the drive. However, the disk drive is a digitally sampled system with inherent computational delay in the control electronics. Both the computational delay and the delay due to sampling result in the phase loss shown in the measured transfer functions. The HSA model presented in this paper is a continuous model and does not account for any delay terms.

Another method to achieve the correct frequency response for the two rigid body modes, is to express the 2-DOF HSA model as a fourth order transfer function. The HSA is a good example of a non-collocated system, where there is a flexible mechanical member (pivot bearings) between the actuator (coil) and the sensor (read/write head). Non-collocated systems accounting for one mechanical resonance can be modeled as a fourth order system by the following normalized transfer function

$$G(s) = \frac{K}{s^2 \left(\frac{s^2}{\omega_n^2} + \frac{2\xi s}{\omega_n} + 1 \right)} \quad (5-6)$$

where

$$\omega_n = \sqrt{\frac{K_{bearing}}{M_T}} \quad \text{and} \quad K = \frac{K_t R_h}{J_T} K_{BW} \quad (5-7)$$

From Figure 5-4 below, it can be seen that the non-located transfer function of

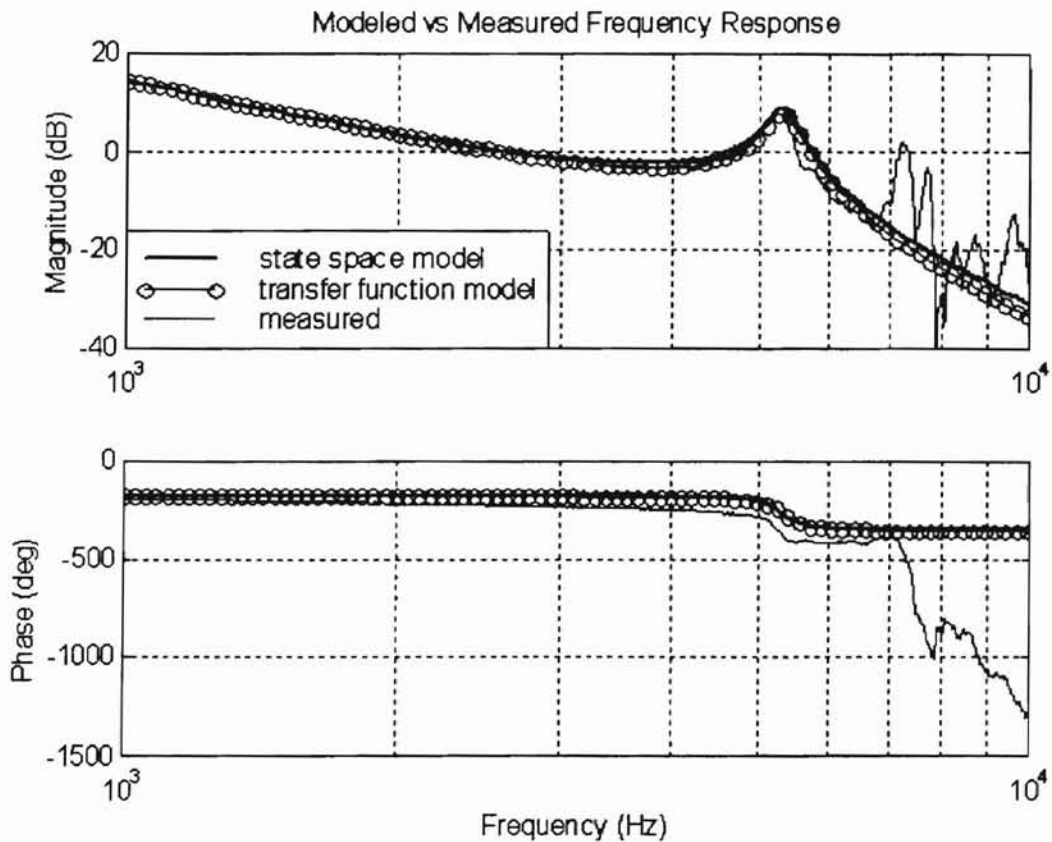


Figure 5-4: Non-Collocated Transfer Function vs. Measured Frequency Response

equation (5-6) matches the measured data and the corrected state space model. The transfer function can be easily transformed into an equivalent state space model using Matlab so that the rigid body model can be used with the HSA model previously

developed. However, for the full order model simulation results presented below, the gain adjusted state space model is used.

5.2 Full Order Model Simulation

The full order model includes sub-component flexible modes and is a 15 DOF model. The model consists of 2 rigid body modes, 3 yoke modes, 4 arm modes, and 6 suspension modes. The flexible modes that are included in the model are those resonances whose mode shapes have displacement in the off-track direction or have the potential to cause displacement in the off-track direction. The Matlab script file used in the simulation is shown in Appendix D.

HSA modes can be identified as either in-plane or out-of-plane resonances. In-plane resonances are resonances in which the motion of the structure is primarily in the plane of the disk. The resulting motion of the slider due to in-plane resonances is radial off-track motion. From an analytical point of view, these modes can be modeled as a complex pole pair. Examples of in-plane resonances that will be considered in the HSA model are the bearing translational mode and the sway modes of the arm, suspension, and yoke. Out-of plane resonances are resonances in which the motion of the structure is primarily perpendicular to the plane of the disk. In order for these modes to modify the open loop or structural response, there must be some amount of radial or off-track motion associated with the mode shape. Ideally, out-of-plane resonances would not add to the off-track motion of the slider. However, unless the slider is at a nodal point of the mode shape, out-of-plane modes will usually exhibit some amount off-track motion. Out-of-plane modes can typically be modeled as complex pole/zero pairs. Examples of

out-of-plane resonances that will be considered in the HSA model are bending and torsion modes of the arm, suspension, and yoke.

The zeros associated with out-of-plane resonances make it difficult to accurately model the off-track displacements. The relationship of the zeros and the poles determine the magnitude and phase response of out-of-plane resonances. Slight differences in arm or suspension geometry or time and temperature effects that can change the mode shape and make the off-track displacements due to out-of-plane modes vary greatly from drive to drive.

The results of the initial simulation of the sub-component FE analytical model can

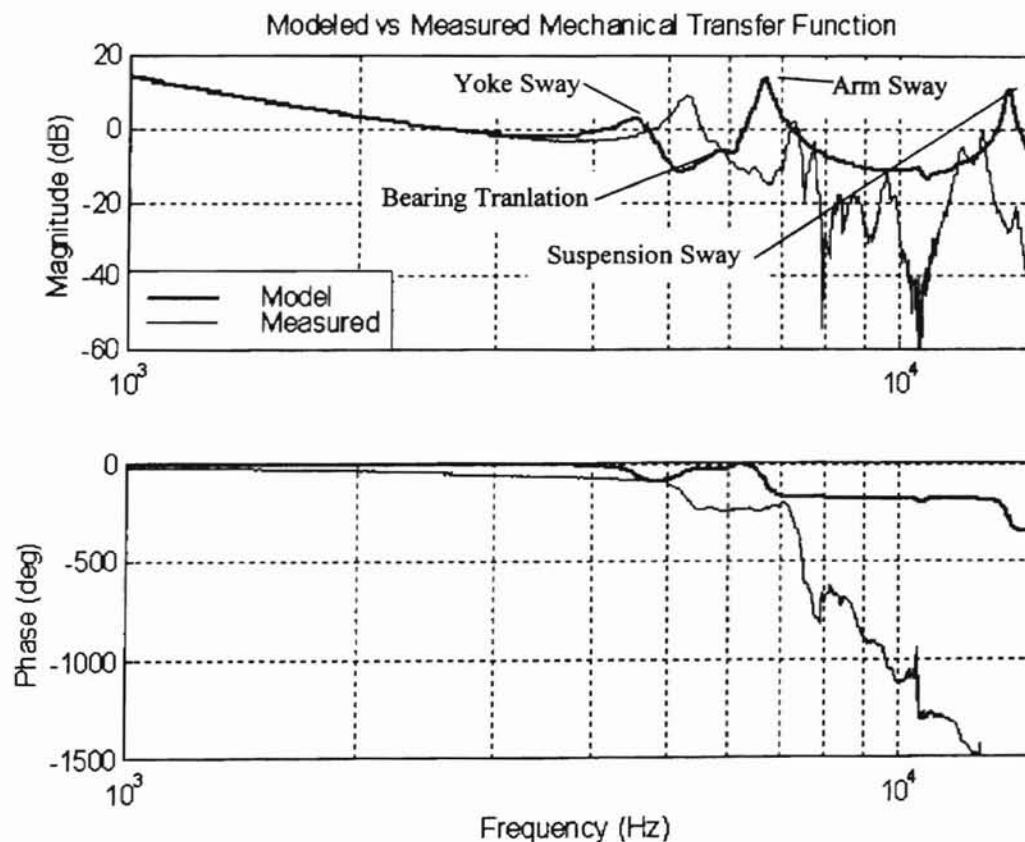


Figure 5-5: Initial Simulation of the Sub-Component FE Analytical Model

be seen in Figure 5-5 compared with data from a measured drive. As can be seen in Figure 5-5, there are several differences between the measured and modeled data

resulting primarily from the sway modes of the yoke, arm and suspension. The modal participation factors (Γ) and modal displacements (ϕ) for these three modes are approximately two times the desired magnitude. The appropriate values for the modal participation factors and modal displacements are determined by iterating on these terms in the sub-component FE model until the model converges with the measured data. By

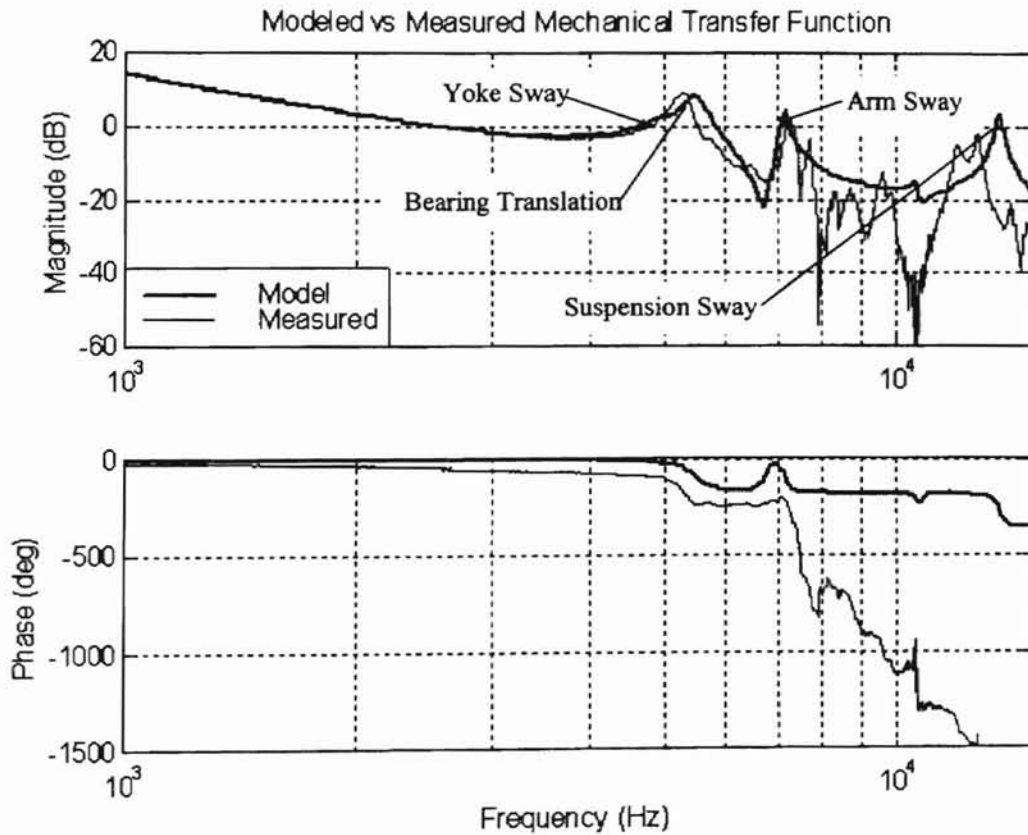


Figure 5-6: Sub-Component FE Model Simulation with Corrected Sway Mode Coupling Factors

reducing the modal displacements and coupling factors of the three sway modes by a factor of two, the modeled frequency response agrees much more closely with the measured data as seen in Figure 5-6. The remaining differences between the modeled and measured transfer functions in Figure 5-6 result from two primary sources. First, the natural frequencies of the sub-component FE models can differ from measured data by

approximately 7% as previously discussed. Second, out-of-plane modes (bending and torsion modes) do not exhibit sufficient off-track displacements in the sub-component FE models.

The differences between the modeled and measured frequency response functions arise from errors in the sub-component FE models. Errors in the FE model results can be due to incorrect boundary conditions and incorrect assumptions and simplifications regarding the modeled part. For example, when parts are modeled using FE models, the part is typically assumed to be a nominal part and tolerances are not considered. However, all parts deviate from nominal manufacturing values. Due to the increasing TPIs and the corresponding decrease in track widths, displacement of the slider of only a few micro-inches can be detrimental to drive performance. As a result, part tolerances can have a significant impact on the dynamic performance of the HSA. Slight bends, twists, or asymmetries that arise due to part tolerances can change the mode shape so that the resulting off-track motion for a given mode is reduced or increased. The HSA model that has been developed is only as accurate as the sub-component FE models.

One of the greatest advantages of the HSA model developed in this paper is that it that it can be used to provide direction for improving the sub-component FE models. The sub-component FE analytical model that has been developed is a compact model that can be used to determine the appropriate modal participation and displacement values so that the model matches measured data. The new values obtained from the HSA model can be used to improve the accuracy and reliability of the FE models. As an example, the appropriate modal parameters (Γ and ϕ) were determined using the sub-component FE model for the 3rd bending mode of the suspension such that the modeled

frequency response matched the measured frequency response for the mode of concern. Using the new Γ and ϕ modal parameters as target values, the suspension sub-component FE model was modified until the appropriate modal participation factor and mode shape value for the 3rd bending mode matched the values dictated by the sub-component FE analytical model. The necessary changes to the suspension FE model included twisting the suspension two degrees and adding the copper runs that carry the read/write signal to and from the head. The added twist to the suspension approximates the handling and assembly tolerances that allow for a slightly imperfect suspension and the copper runs add an asymmetrical mass loading to the suspension. The differences in the un-modified and modified 3rd bending mode of the suspension can be seen in Figures 5-7 and 5-8. In

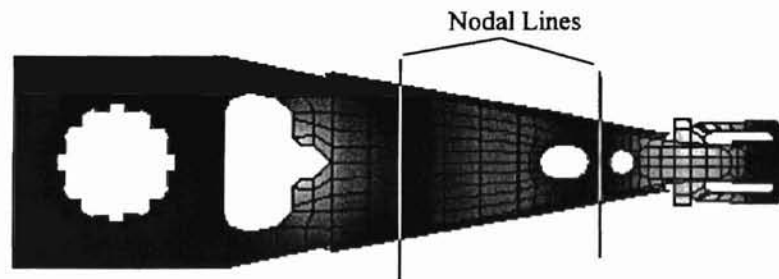


Figure 5-7: Original Suspension 3rd Bending Mode

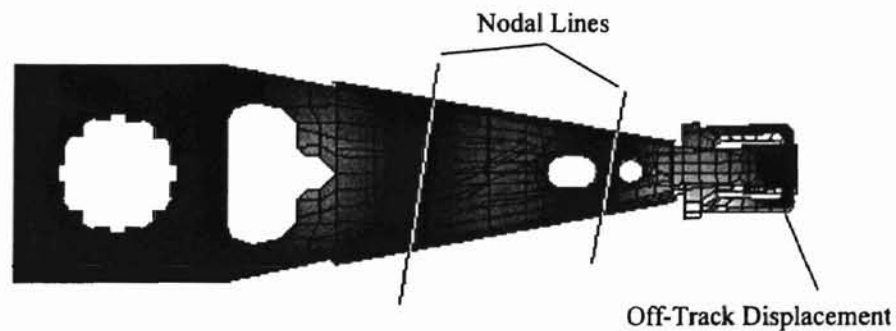


Figure 5-8: Modified Suspension 3rd Bending Mode

Figure 5-7, the nodal lines are perpendicular to the center line of the suspension, resulting in little or no off-track displacement of the slider due to the 3rd bending mode.

However, in Figure 5-8, the nodal lines are an angle to the suspension center line as a result of the modifications that were made, so that the slider will exhibit off-track motion associated with the 3rd bending mode. The resulting changes that were required for the 3rd bending mode, show that the assumptions and simplifications used to create original suspension FE were incorrect.

By decreasing the sway mode coupling factors, adjusting the natural frequencies to account for modeling/measurement differences, and correcting the sub-component FE models so that out-of-plane modes exhibit sufficient off-track displacements, the sub-component FE analytical model shows good agreement with measured data as shown in Figure 5-9. The only significant discrepancies that remain between the modeled and

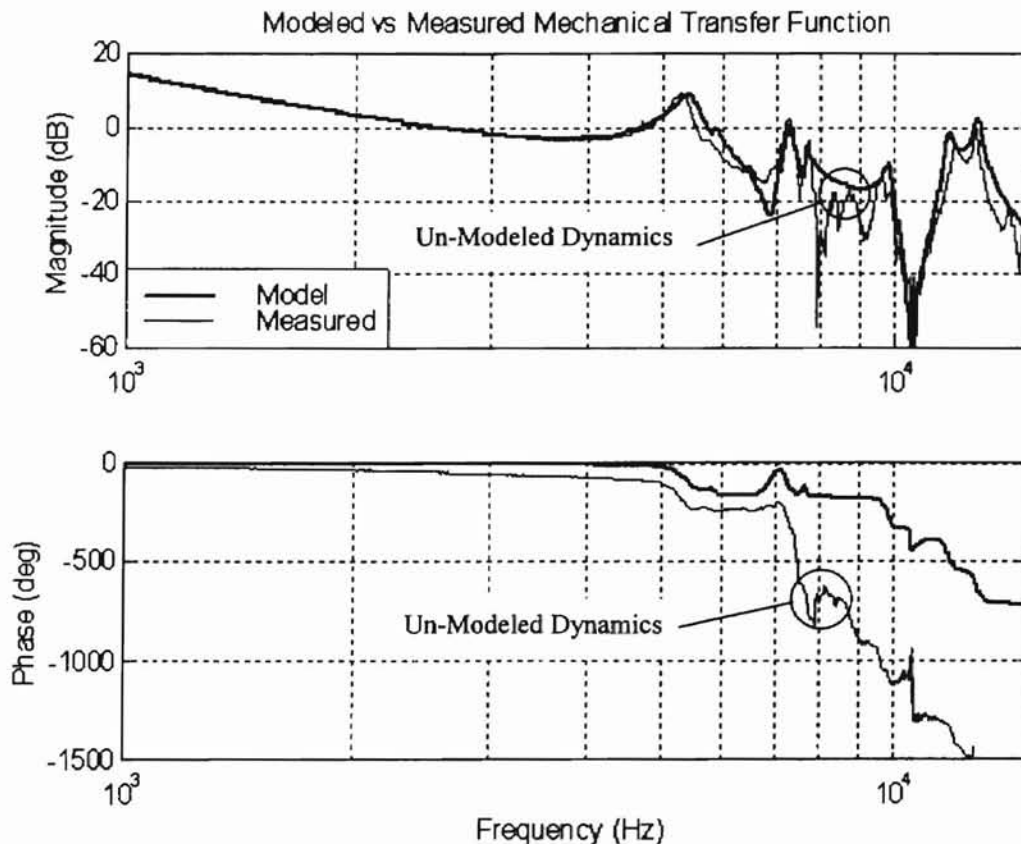


Figure 5-9: Modified Sub-Component FE Analytical Model Simulation

measured data are due to un-modeled dynamics between 8 kHz and 9 kHz. The yoke/coil, arm, and suspension sub-component FE models do not predict flexible mechanical resonances between 8 kHz and 9 kHz. These modes are possibly system modes where all of the sub-components contribute significantly to the overall mode shape or coupled modes where multiple arms and suspensions deform together as a group. In the case of coupled modes, the arms or suspensions of the HSA appear to be coupled together since they deform simultaneously in similar mode shapes. Typically patterns are established such that one coupled mode might involve every other arm of the HSA at a particular frequency, while at a different frequency, the inner arms might deform as a group out-of-phase with the outer arms. However, since the sub-component FE analytical model only considers one arm and suspension, and not the entire HSA, the model will not predict system or coupled modes.

6 Conclusions and Future Work

6.1 Conclusions

The resulting sub-component finite element analytical model was a 15 degree of freedom model that could quickly be solved using commercially available matrix manipulation software. The model proved to be accurate in predicting the off-track motion of the head stack assembly and helped provide understanding as to which resonances are the most detrimental to drive performance. Initial simulations showed that some of the boundary conditions and assumptions used in creating the sub-component finite element models were incorrect. Due to modeling errors in the sub-component FE models, the off-track amplitude and coupling factors of the in-plane sway modes were approximately two times the desired magnitude. Conversely, the amplitude and coupling factors of the out-of-plane modes were not of sufficient magnitude. However, by comparing the model results to measured data, the sub-component finite element analytical model provided direction to help improve the accuracy of the individual sub-component models, as was demonstrated with the 3rd bending mode of the suspension. Also, since coupling terms were derived that describe how the sub-components interact to form the overall system dynamics, the sub-component finite element analytical model can provide direction to help optimize the head stack assembly design in order to reduce the impacts of mechanical resonances.

6.2 Future Work

One of the main advantages of the HSA model developed in this paper, is that it provides a means to predict track following performance in advance of a working drive. However, without the servo control loop, only the mechanical interactions between the yoke, pivot bearings, arm, and suspension can be studied with the current HSA model. It would be very beneficial to include the control loop so that the effects of HSA resonances on servo stability could be investigated as well. By adding the servo control loop, the HSA model could be used to study drive performance impacts for new actuator and suspension designs in the presence of increasing TPI as well as provide a platform for theoretical compensator design work.

Another area of work that needs to be furthered is an investigation as to the correct boundary conditions and assumptions to be used for the sub-component FE models. Specifically, the cause of the excessive displacement amplitudes associated with the sway modes and the insufficient displacement amplitudes associated with the out-of-plane modes needs to be understood so that accurate sub-component FE models can be generated. As previously mentioned, the sub-component FE analytical model is only as accurate as the sub-component models.

Lastly, no drives are identical. Each drive has a unique frequency response function due to differences in each HSA caused by manufacturing and assembly tolerances. These differences result in drive to drive variations in the natural frequencies and amplitudes of the in-the-loop resonances. The off-track displacement amplitudes of out-of-plane resonances are particularly susceptible to variations in the HSA due to the zeros that are associated with these modes. In order represent the variations in the

frequency response that might be expected over a large population of drives, the HSA model can be used to generate probabilistic distribution of transfer functions by using a statistical sampling method. One such method is often referred to as a Monte Carlo analysis where each variable in the model is assumed to have a statistical distribution. For the HSA model, the off-track amplitude and natural frequency distribution for each mode would best be obtained by measuring a large sample of drives. Using a Monte Carlo analysis, numerous HSA transfer functions could be generated by randomly selecting natural frequency, modal participation, and mode shape values from the corresponding distribution functions. Once all the transfer functions have been calculated, a minimum and maximum "envelope" transfer function can be determined that would represent a range of values that a population of drives should fall within.

REFERENCES

1. Aruga, K., Kuroba, Y., Koganezawa, S., Yamada, T., Nagasawa, Y., Komura, Y., "High-Speed Orthogonal Power Effect Actuator for Recording at Over 10,000 TPI," *IEEE Transactions on Magnetics*, Vol. 32, No. 3, May 1996, pp. 1756-1761.
2. Chiou, S. S., Miu, D. K., "Tracking Dynamics of In-line Suspension in High-Performance Rigid Disk Drives with Rotary Actuators," *ASME Journal of Vibration and Acoustics*, Vol. 114, January 1992, pp. 67-73.
3. Evans, R., Carlson, P., Messner, W., "Two-Stage Microactuator Keeps Disk Drive on Track," *Data Storage*, April 1998, pp. 43-44.
4. Franklin, G. F., Powell, J. D., Workman, M. L., *Digital Control of Dynamic Systems*, 3rd ed., Addison-Wesley, Inc., Reading, MA, 1998, pp. 649-687.
5. Hewlett-Packard, *The Fundamentals of Modal Testing Application Note 243-3*, Hewlett-Packard Co., Palo Alto, California, 1986.
6. Jeans, A. H., "Analysis of the Dynamics of a Type 4 Suspension," *ASME Journal of Vibration and Acoustics*, Vol. 114, January 1992, pp. 74-78.
7. Miu, D. K., "Physical Interpretation of Transfer Function Zeros for Simple Control Systems with Mechanical Flexibilities," *Robotics Research*, Vol. 26, 1990, pp. 67-73.
8. Miu, D. K., Frees, G. M., Gompertz, R. S., "Tracking dynamics of Read/Write Head Suspension in High-Performance Small Form Factor Rigid Disk Drives," *ASME Journal of Vibration and Acoustics*, Vol. 112, January 1990, pp.33-39.
9. Miu, D. K., Yang, B., "On Transfer Function Zeros of General Colocated Control Systems with Mechanical Flexibilities," *ASME Journal of Dynamic Systems, Measurement, and Control*, Vol. 116, March 1994, pp. 151-154.
10. Ono, K., Teramoto, T., "Design Methodology to Stabilize the Natural modes of Vibration of a Swing-Arm Positioning Mechanism," *Advances in Information Storage Systems*, Vol. 4, 1992, pp. 343-359.

11. Radwan, H. R., Huang, F., Serrano, J., Oettinger, E., "Control-Structure Interaction in Disk Drives Using Modal Superposition and Finite-Element Analysis," *Journal of Information Storage and Processing Systems*, Vol. 1, 1999, pp. 87-94.
12. Radwan, H. R., Phan, D. T., Cao, K., "Effect of disk Drive Actuator Unbalance on Track Following Response to External Vibration and Shock," *IEEE Transactions on Magnetics*, Vol. 32, No. 3, May 1996, pp. 1749-1755.
13. Radwan, H. R., Whaley, R., "Servo-Structure Interaction in Disk Drives Using Finite Element Analysis," *ASME Advances in Information Storage Systems*, Vol. 5, 1993, pp.101-118.
14. Spanos, J. T., "Control-Structure Interaction in Precision Pointing Servo Loops," *Journal of Guidance*, Vol. 12, No. 2, March-April 1989, pp. 256-263.
15. Wilson, C. J., Bogy, D. B., "Experimental Modal Analysis of a Suspension Assembly Loaded on a Rotating Disk," *ASME Journal of Vibration and Acoustics*, Vol. 116, January 1994, pp. 85-92.

APPENDIX A



Figure A-1: Suspension 1st Bending



Figure A-2: Suspension 1st Torsion



Figure A-3: Suspension 2nd Bending

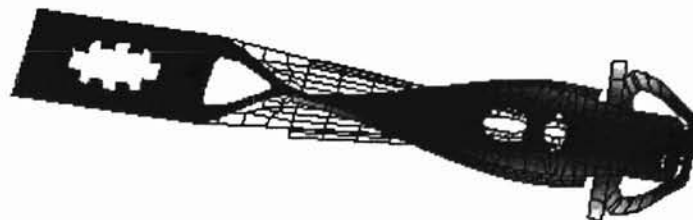


Figure A-4: Suspension 2nd Torsion



Figure A-5: Suspension 3rd Bending

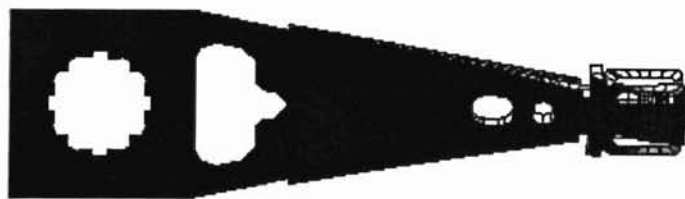


Figure A-6: Suspension Sway

APPENDIX B

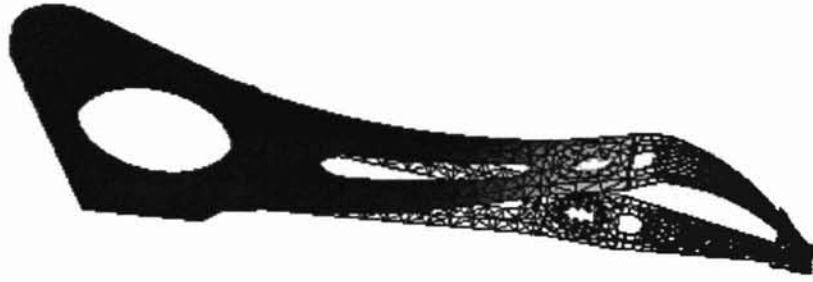


Figure B-1: Arm 1st Bending

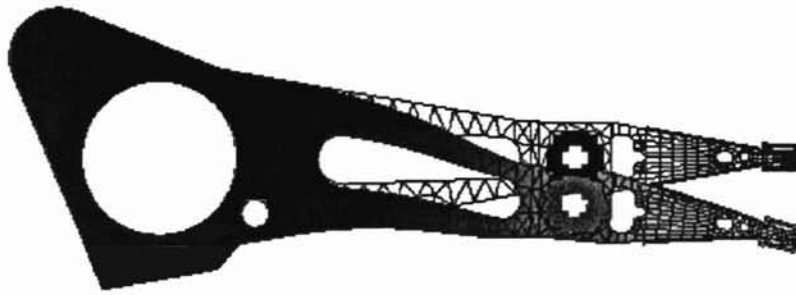


Figure B-2: Arm Sway



Figure B-3: Arm 2nd Bending



Figure B-4: Arm 1st Torsion

APPENDIX C

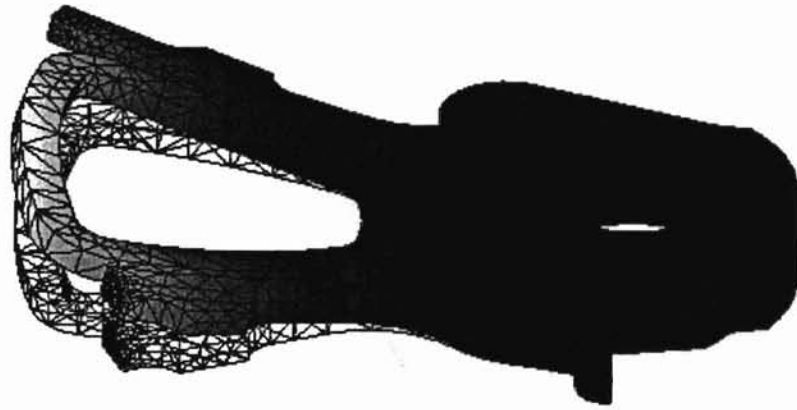


Figure C-1: Yoke/Coil 1st Bending

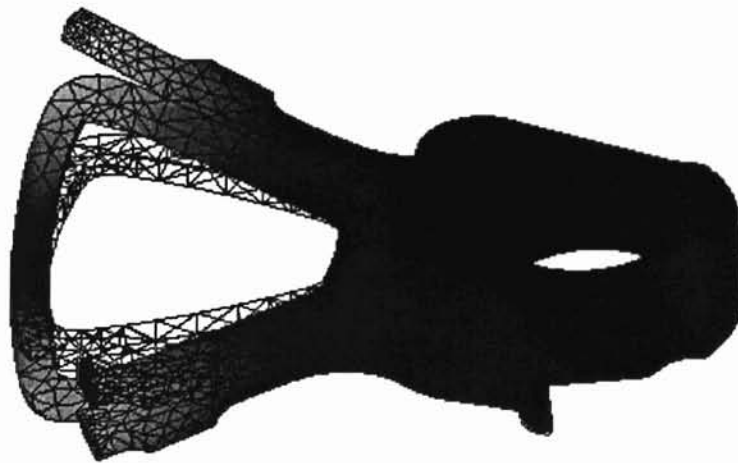


Figure C-2: Yoke/Coil 1st Torsion

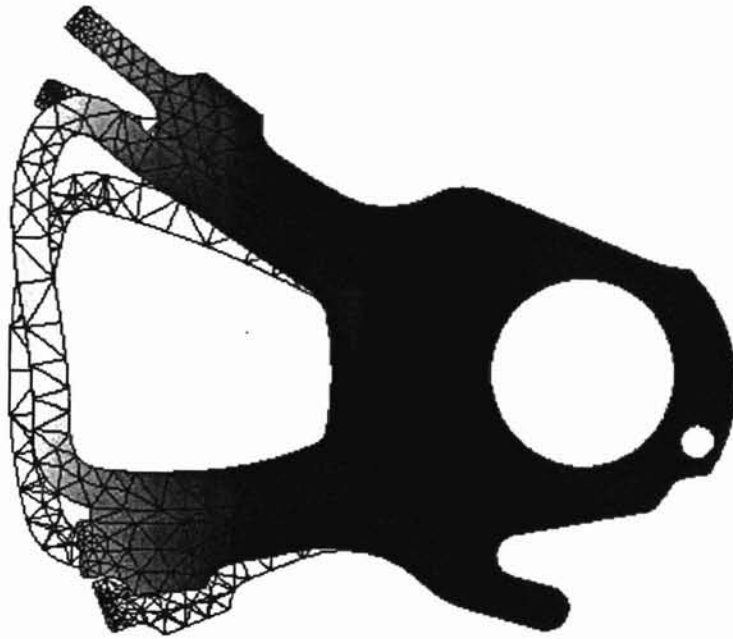


Figure C-3: Yoke/Coil Sway

APPENDIX D

```

function [mag,phase,freq]=actmod
%%%%%%%%%%%%%%%%%%%%%%%%%%%%%%%%%%%%%%%%%%%%%%%%%%%%%%%%%%%%%%%%%%%%%%%%
%
%   Sub-Component FE Analytical HSA Model
%
%   Written by:  Jeff Andress
%               1/17/99
%
%%%%%%%%%%%%%%%%%%%%%%%%%%%%%%%%%%%%%%%%%%%%%%%%%%%%%%%%%%%%%%%%%%%%%%%%

%%%%%%%%%%%%%%%%%%%%%%%%%%%%%%%%%%%%%%%%%%%%%%%%%%%%%%%%%%%%%%%%%%%%%%%%
%   Model Parameters
%%%%%%%%%%%%%%%%%%%%%%%%%%%%%%%%%%%%%%%%%%%%%%%%%%%%%%%%%%%%%%%%%%%%%%%%

%%%%%% Rigid Body Parameters %%%%%%%%%

Mt=13.5/454/386; %total actuator mass (lbf-s^2/in)
Kbrg=90000;      %bearing stiffness (lbf/in)
J=0.00037/16;   %actuator inertia about pivot (lbf-in-s^2)
Rhead=1.80;     %pivot to gap distance (in)
Rcoil=.85;      %coil c.g. to pivot distance (in)
Kt=9.6/16;      %torque constant (lbf-in/Amp)
TPI=18145;      %tracks/inch
vpt=5;          %volts/track
Kbw=.0455;      %bandwidth adjustment factor to compensate
                %for gain of drive electronics

%%%%%%%%%%%%%%%%%%%%%%%%%%%%%%%%%%%%%%%%%%%%%%%%%%%%%%%%%%%%%%%%%%%%%%%%

%%%%%%%%%%%%%%%%%%%%%%%%%%%%%%%%%%%%%%%%%%%%%%%%%%%%%%%%%%%%%%%%%%%%%%%%
%   Model Parameters from FEM Analysis
%
%   p=normal mode (normalized by modal mass)
%   mm=modal mass
%   g=modal participation factor
%
%%%%%%%%%%%%%%%%%%%%%%%%%%%%%%%%%%%%%%%%%%%%%%%%%%%%%%%%%%%%%%%%%%%%%%%%

%%%%%% FEM Yoke Parameters: %%%%%%%%%

my=2.57e-5; %total mass of the yoke/coil FE model

%%% Mode 1: Yoke 1st Bending %%%
wyl=1124*2*pi;
mmy1=3.52826e-3;
pyl=(9.8118e-3+4.0265e-3)/sqrt(mmy1);
gyl=sqrt(0.0*my);

%%% Mode 2: Yoke Torsion %%%
wy2=1821*2*pi;
mmy2=2.95827e-3;
py2=(3.0722e-2+7.0812e-3)/sqrt(mmy2);
gy2=sqrt(0.0*my);

%%% Mode 3: Yoke Sway %%%
wy3=5068*2*pi;

```

```
mmy3=4.93233e-3;
py3=(1.469e1+1.3564e1)/sqrt(mmy3)/2;
gy3=sqrt(0.0087117*my)/2;
```

```
%%%%%%%%%%%%%%%%%%%%%%%%%%%%%%%%%%%%%%%%%%%%%%%%%%%%%%%%%%%%%%%%%%%%%%%%
```

```
%%%%%%%% FEM Arm Parameters: %%%%%%%%%
```

```
mas=6.133e-6; %total mass of the arm FE model
```

```
%%% Mode 1: Arm 1st Bending %%%
```

```
wal=1079*2*pi;
mmal=1.21434e-8;
pal=4.9603e-6/sqrt(mmal);
gal=sqrt(0*mas);
```

```
%%% Mode 2: Arm 2nd Bending %%%
```

```
wa2=7508*2*pi;
mma2=4.411692e-10;
pa2=4.8836e-5/sqrt(mma2);
ga2=sqrt(0.000001*mas);
```

```
%%% Mode 3: Arm Sway %%%
```

```
wa3=7240*2*pi;
mma3=1.10235e-7;
pa3=-3.1594e-1/sqrt(mma3)/3;
ga3=sqrt(0.216352*mas);
```

```
%%% Mode 4: Arm 1st Torsion %%%
```

```
wa4=7600*2*pi;
mma4=6.50653e-10;
pa4=-1.3948e-4/sqrt(mma4);
ga4=sqrt(0.05*mas);
```

```
%%%%%%%%%%%%%%%%%%%%%%%%%%%%%%%%%%%%%%%%%%%%%%%%%%%%%%%%%%%%%%%%%%%%%%%%
```

```
%%%%%%%% FEM Suspension Parameters: %%%%%%%%%
```

```
mst=2.6999e-7; %total mass of suspension FE Model
```

```
%%% Mode 1: Suspension 1st Bending %%%
```

```
ws1=1970*2*pi;
mms1=2.66717e-10;
ps1=5.0782e-4/sqrt(mms1);
gs1=sqrt(0.000042*mst);
```

```
%%% Mode 2: Suspension 1st Torsion %%%
```

```
ws2=4200*2*pi;
mms2=3.80279e-11;
ps2=-3.2672e-3/sqrt(mms2);
gs2=sqrt(0.000116*mst);
```

```
%%% Mode 3: Suspension 2nd Bending %%%
```

```
ws3=5820*2*pi;
mms3=4.68809e-11;
```

```
ps3=-1.0129e-3/sqrt(mms3)*2;
gs3=sqrt(0.0215*mst);
```

```
%%% Mode 4: Suspension 2nd Torsion %%%
ws4=9800*2*pi;
mms4=9.73791e-12;
ps4=-3.1100e-3/sqrt(mms4);
gs4=sqrt(0.00695*mst);
```

```
%%% Mode 5: Suspension 3rd Bending %%%
ws5=11770*2*pi;
mms5=1.43310e-11;
ps5=6.2329e-3/sqrt(mms5);
gs5=sqrt(0.06*mst);
```

```
%%% Mode 6: Suspension Sway %%%
ws6=12830*2*pi;
mms6=1.01493e-12;
ps6=4.1307e-3/sqrt(mms6)/2;
gs6=sqrt(0.156*mst);
```

```
%%%%%%%%%%%%%%%%%%%%%%%%%%%%%%%%%%%%%%%%%%%%%%%%%%%%%%%%%%%%%%%%%%%%%%%%
% Form Mass Matrix
%%%%%%%%%%%%%%%%%%%%%%%%%%%%%%%%%%%%%%%%%%%%%%%%%%%%%%%%%%%%%%%%%%%%%%%%
```

```
m=[Mt 0 gy1 gy2 gy3 gal+mst*pa1 ga2+mst*pa2 ga3+mst*pa3 ga4+mst*pa4 gs1
gs2 gs3 gs4 gs5 gs6;
0 J 0 0 0 0 0 0 0 0 0 0 0 0 0;
gy1 0 1 0 0 0 0 0 0 0 0 0 0 0 0;
gy2 0 0 1 0 0 0 0 0 0 0 0 0 0 0;
gy3 0 0 0 1 0 0 0 0 0 0 0 0 0 0;
gal+mst*pa1 0 0 0 0 1+mst*pa1*pa1 mst*pa1*pa2 mst*pa1*pa3 mst*pa1*pa4
gs1*pa1 gs2*pa1 gs3*pa1 gs4*pa1 gs5*pa1 gs6*pa1;
ga2+mst*pa2 0 0 0 0 mst*pa1*pa2 1+mst*pa2*pa2 mst*pa2*pa3 mst*pa2*pa4
gs1*pa2 gs2*pa2 gs3*pa2 gs4*pa2 gs5*pa2 gs6*pa2;
ga3+mst*pa3 0 0 0 0 mst*pa1*pa3 mst*pa3*pa2 1+mst*pa3*pa3 mst*pa3*pa4
gs1*pa3 gs3*pa3 gs4*pa3 gs4*pa3 gs5*pa3 gs6*pa3;
ga4+mst*pa4 0 0 0 0 mst*pa1*pa4 mst*pa4*pa2 mst*pa4*pa3 1+mst*pa4*pa4
gs1*pa4 gs3*pa4 gs4*pa4 gs4*pa4 gs5*pa4 gs6*pa4;
gs1 0 0 0 0 gs1*pa1 gs1*pa2 gs1*pa3 gs1*pa4 1 0 0 0 0 0;
gs2 0 0 0 0 gs2*pa1 gs2*pa2 gs2*pa3 gs2*pa4 0 1 0 0 0 0;
gs3 0 0 0 0 gs3*pa1 gs3*pa2 gs3*pa3 gs3*pa4 0 0 1 0 0 0;
gs4 0 0 0 0 gs4*pa1 gs4*pa2 gs4*pa3 gs4*pa4 0 0 0 1 0 0;
gs5 0 0 0 0 gs5*pa1 gs5*pa2 gs5*pa3 gs5*pa4 0 0 0 0 1 0;
gs6 0 0 0 0 gs6*pa1 gs6*pa2 gs6*pa3 gs6*pa4 0 0 0 0 0 1];
```

```
%%%%%%%%%%%%%%%%%%%%%%%%%%%%%%%%%%%%%%%%%%%%%%%%%%%%%%%%%%%%%%%%%%%%%%%%
% Form Stiffness Matrix
%%%%%%%%%%%%%%%%%%%%%%%%%%%%%%%%%%%%%%%%%%%%%%%%%%%%%%%%%%%%%%%%%%%%%%%%
```

```
temp=[Kbrg 0 wy1^2 wy2^2 wy3^2 wal^2 wa2^2 wa3^2 wa4^2 ws1^2 ws2^2
ws3^2 ws4^2 ws5^2 ws6^2];
k=diag(temp,0);
```

```
%%%%%%%%%%%%%%%%%%%%%%%%%%%%%%%%%%%%%%%%%%%%%%%%%%%%%%%%%%%%%%%%%%%%%%%%
% Form Input Array
```

```

%%%%%%%%%%%%%%%%%%%%%%%%%%%%%%%%%%%%%%%%%%%%%%%%%%%%%%%%%%%%%%%%%%%%%%%%
f=Kt/Rcoil*[Mt*Rhead/J Rcoil py1/2 py2/2 py3/2 0 0 0 0 0 0 0 0 0 0 0]';

%%%%%%%%%%%%%%%%%%%%%%%%%%%%%%%%%%%%%%%%%%%%%%%%%%%%%%%%%%%%%%%%%%%%%%%%
%      Form State Space
%%%%%%%%%%%%%%%%%%%%%%%%%%%%%%%%%%%%%%%%%%%%%%%%%%%%%%%%%%%%%%%%%%%%%%%%

za=0.005;    %damping ratio for the arm modes
zs=0.01;    %damping ratio for the suspension modes
zy=0.01;    %damping ratio for the yoke modes

a=zeros(30,30);
temp(1:15)=1;;
a(1:15,16:30)=diag(temp,0);
a(16:30,1:15)=-(inv(m)*k);
temp=[-2*0.03*sqrt(Kbrg/Mt) 0 -2*zy*wy1 -2*zy*wy2 -2*.05*wy3 -2*za*wa1
-2*za*wa2 -2*.01*wa3 -2*za*wa4 -2*zs*ws1 -2*zs*ws2 -2*zs*ws3 -
2*0.01*ws4 -2*zs*ws5 -2*zs*ws6];
a(16:30,16:30)=diag(temp,0);

b(1:15,1)=0;
b(16:30)=inv(m)*f;

c=[1 -Rhead 0 0 0 0 0 0 0 -ps1 -ps2 ps3 -ps4 -ps5 ps6];
c(16:30)=0;
d=0;

input=100*2*pi:5*2*pi:15000*2*pi;    %frequency range for bode plot

if nargout==0

%%%%%%%%%%%%%%%%%%%%%%%%%%%%%%%%%%%%%%%%%%%%%%%%%%%%%%%%%%%%%%%%%%%%%%%%
%
%  load measured data for comparison
%
%%%%%%%%%%%%%%%%%%%%%%%%%%%%%%%%%%%%%%%%%%%%%%%%%%%%%%%%%%%%%%%%%%%%%%%%

load c:\matlab\toolbox\user\measmag.txt;
load c:\matlab\toolbox\user\measph.txt;
load c:\matlab\toolbox\user\freq.txt;

[mag2,phase2,freq2]=bode(a,b,c,d,1,input);
mag2=mag2*TPI*vpt*Kbw;

subplot(2,1,1)
handle1=semilogx(freq2/(2*pi),20*log10(mag2),'k',freq,measmag,'k');
grid;
maxy=max(20*log10(mag2))+10;
miny=min(20*log10(mag2))-10;
axis([1000 15000 -60 20]);
ylabel('Magnitude (dB)');
title('Modeled vs Measured Mechanical Transfer Function');

subplot(2,1,2)
handle2=semilogx(freq2/(2*pi),phase2,'k',freq,measph,'k');
grid;

```

```
axis([1000 15000 -1500 10]);
ylabel('Phase (deg)');
xlabel('Frequency (Hz)');
set(handle1(1), 'LineWidth', 2);
set(handle2(1), 'LineWidth', 2);
legend('Model', 'Measured');

else

[mag, phase, freq]=bode(a,b,c,d,1,input);
freq=freq/(2*pi);
mag=mag*TPI*vpt*Kbw;

end
```

VITA

Jeffrey Don Andress

Candidate for the Degree of

Master of Science

Thesis: DYNAMIC MODELING OF A HARD DISK DRIVE ACTUATOR USING
SUB-COMPONENT FINITE ELEMENT MODELS AND MODAL
SUPERPOSITION

Major Field: Mechanical Engineering

Biographical:

Education: Graduated from Bartlesville High School, Bartlesville, Oklahoma in May 1989. Received Bachelor of Science Degree in Mechanical Engineering from Oklahoma State University, Stillwater, Oklahoma in December 1994. Completed requirements for the Master of Science Degree in Mechanical Engineering at Oklahoma State University in May 2000.

Professional Experience: Worked as a Mechanical Design Engineer for Seagate Technology, Oklahoma City, Oklahoma 1995 to present.